공학박사학위논문

Method of LSPR and SERS Simultaneous Detection for Bio-applications: On Optical System and Sensor Substrate

바이오 응용을 위한 LSPR 과 SERS 동시측정방법: 광학 시스템과 센서 기판에 대해서

2017 년 2 월

서울대학교 대학원
협동과정 나노과학기술전공
노로에르덴

Dissertation for the Degree of Doctor of Engineering

Method of LSPR and SERS Simultaneous Detection for Bio-applications: On Optical System and Sensor Substrate

February, 2017

by

Norov Erdene

Interdisciplinary Program in Nano-Science and Technology
Graduate School of Seoul National University

Method of LSPR and SERS Simultaneous Detection for Bio-applications: On Optical System and Sensor Substrate

지도교수 : 정대홍

이 논문을 공학박사 학위 논문으로 제출함

2016 년 6 월

서울대학교 대학원

협동과정 나노과학기술전공

노로에르덴

노로에르덴의 공학박사 학위논문을 인준함

2017 년 2 월

위 원 장	김 연 상	(인)
부위원장	정 대 홍	(인)
위 원	이 호 영	(인)
위 원	박 재 형	(인)
위 원	이 상 명	(인)

ABSTRACT

Method of LSPR and SERS Simultaneous Detection for Bio-Applications: On Optical System and Sensor Substrate

(Supervisor: Dae Hong Jeong, Ph.D)

Norov Erdene

Interdisciplinary Program in Nano-Science and Technology

College of Natural Science

Graduate School of Seoul National University

In a field of bio-molecular analysis, various kinds of biosensors have been developed extensively. Each of them has many benefits and variations in the instrument designs. In this study proposed is a fiber optic (FO) sensor which has many advantages such as utilization of localized surface Plasmon resonance (LSPR) and surface enhanced Raman scattering (SERS) simultaneously and real time detection of antibody-antigen reaction. The fiber optic sensors were successfully utilized as label-free LSPR and SERS simultaneous detection of antibody-antigen reaction interferon-gamma (IFN-γ) as a proof-of-concept for bio-related applications.

Chapter I, as an introductory chapter, aims to provide a brief theoretical information, basic principles and research objective of this study. Also

modern techniques that are broadly used in field of bio-molecular detection and its examples are discussed.

In Chapter II, fabrication of the FO LSPR and SERS sensor and its simultaneous detection system for bio-applications were described. First, an FO sensor was fabricated by immobilizing gold nanoparticles (Au NPs, *ca.* 50±5nm diameter) on one end of a fiber optic by chemical reaction. And simultaneous detection system of the LSPR and SERS was assembled. Then, for checking the FO sensor quality, sensitivity, and also simultaneous detection system reliability, LSPR and SERS signals were measured using various refractive indices solutions and SERS reporter molecule of 4-aminothiphenol (ATP). Finally, the sensor was applied to observe real-time LSPR sensor-gram and SERS spectra of the reporter molecule of ATP during the antibody-antigen reaction of interferon-gamma (IFN-γ) as experiment of biological applications.

In a variety of practical applications, including surface plasmon resonance (SPR) sensors and surface-enhanced Raman scattering (SERS) sensors for bio-detection, noble metal nanoparticles attached to a glass slide or optical fiber are required for increased sensitivity. In addition to sensitivity, reproducibility is important for practical applications. In this aspect, many approaches such as e-beam lithography, vacuum sputtering,

and wet chemical methods have usually been used for deposition of NPs onto the substrate [1-3]. However, issues such as cost of e-beam method and morphological non-uniformity of wet chemical methods hindered sensitive and reproducible fabrication of the sensor substrate. Recently, several photo-induced methods have been demonstrated to grow silver or gold NPs directly on a glass substrate or fiber optic surface from their aqueous solution. Until now, the morphologies of the photo-induced grown nanoparticles on the substrate have not reached enough uniformity.

In Chapter III, a simple method which grows mono-disperse and uniform silver nanoparticles (Ag NPs) directly onto a silica substrate by light irradiation of silver nitrate solution in a presence of sodium citrate was described. Changing the mixed ratio of amine and non-amine functional groups on the substrate as well as photo-illumination time and concentration of growth solutions, mono-disperse growing of Ag NPs was able to control. After photo-induced growing, substrates are characterized by field emission scanning electron microscopy (FE-SEM) and dark field (DF) microscopy. Finally, mechanism of the photo-induced growing process was described on the basis of the experimental results.

Keywords: Fiber-Optic, Localized Surface Plasmon Resonance, Surface Enhanced Raman Scattering, Simultaneous Detection, Gold Nanoparticles, Silver Nanoparticles, Interferon-Gamma, Photo-Reduced Growth, Mixed Self-Assembled Monolayer, Glass Substrate

Student Number: 2006-30675

TABLE OF CONTENTS

Chapter I.

Introduction

Chapter II.

Fiber-Optic Sensor Simultaneously Detecting Localized Surface Plasmon Resonance and Surface-Enhanced Raman Scattering

Chapter III.

Mono-disperse Growth Control of Silver Nanoparticles on Glass Substrate using Photo-reduction and Mixed Self-assembly

LIST OF ABBREVIATIONS

LSPR	localized surface Plasmon resonance
SPR	surface Plasmon resonance
SERS	surface-enhanced Raman scattering
FE-SEM	field emission scanning electron microscopy
DF	dark field microscopy
TEM	transmission electron microscope
NA	numerical aperture
WD	working distance
EDX	energy dispersive X-ray spectroscopy
FO	fiber optic
IFN-γ	interferon-gamma
RI	refractive index
RIU	refractive index unit
RU	resonance unit
SPW	surface Plasmon wave
SP	surface Plasmon
TIR	total internal reflection
NP	nanoparticle
Ag NP	silver nanoparticle

Au NP	gold nanoparticle
4-ATP	4-aminothiophenol
$HAuCl_4$	Gold (III) chloride trihydrate
APMES	3-aminopropyl-dimetylethoxysilan
TMS	methoxytrimethylsilane
BSA	bovine serum albumin
1x PBS	phosphate buffered saline
H_2O_2	hydrogen peroxide
SAM	self-assembled monolayer
CCD	charge-coupled device
DI	deionizied water

LIST OF FIGURES

Chapter I. Introduction

Chapter II. Fiber-Optic Sensor Simultaneously Detecting Localized Surface Plasmon Resonance and Surface-Enhanced Raman Scattering

Chapter III. Mono-disperse Growth Control of Silver Nanoparticles on Glass Substrate using Photo-reduction and Mixed Self-assembly

LIST OF SCHEMES

Chapter I. Introduction

Chapter II. Fiber-Optic Sensor Simultaneously Detecting Localized Surface Plasmon Resonance and Surface-Enhanced Raman Scattering

Chapter III. Mono-disperse Growth Control of Silver Nanoparticles on Glass Substrate using Photo-reduction and Mixed Self-assembly

LIST OF TABLES

Chapter I. Introduction

Chapter II. Fiber-Optic Sensor Simultaneously Detecting Localized Surface Plasmon Resonance and Surface-Enhanced Raman Scattering

No table

Chapter III. Mono-disperse Growth Control of Silver Nanoparticles on Glass Substrate using Photo-reduction and Mixed Self-assembly

No table

Method of LSPR and SERS Simultaneous Detection for Bio-applications: On Optical System and Sensor Substrate

Chapter I.

Introduction

I. Surface Plasmon resonance (SPR) spectroscopy for bio-detection

Surface Plasmon resonance (SPR) is recognized as a powerful concept for refractive index (RI) sensing due to the resonance charge density wave of free electrons in metal film [4, 5]. This phenomenon was first described in the beginning of the twentieth by Wood [6-8]. Later, in 1968 basic optical configuration and excitation of SPR based on method of attenuated total reflection was demonstrated by Kretschmann [9] and Otto [10, 11]. Since then, SPR have been considerably studied and the sensor technology has been developed and commercialized by several companies. The first application of SPR biosensor was demonstrated in 1983 via Lundstrom groups [12] . And BIAcore launched the first SPR biosensor on the market in 1990 [5, 13]. Instead of the BIAcore there are several companies such as Texas Instruments, Quantech, BioTuLBio Instruments, and Xantec Analysensysteme [7, 14], that have been further refined SPR biosensor technology in terms of sensitivity, accuracy, ease of use and cost. Nowadays, SPR has become one of the leading technologies in bio-molecular interactions [7, 15, 16]. It's allowing the real-time analysis of bio-specific interactions without use of labeled molecules [16-19].

In general, SPR-based bio-detection methods have been demonstrated in prism coupler-based biosensors, grating coupler-based biosensors and optical waveguide-based biosensors such as fiber optic (Figure I-1) [15, 20, 21]. Briefly, in these approaches light wave is reflected between prism coupler or grating coupler and metal thin layer interface. Excited surface Plasmon wave (SPW) of the outer boundary of the metal layer evanescently propagate through the layer. And intensity of the reflected light or resonance angle of the incident light is measured. But prism coupler-based biosensors, grating coupler-based biosensors need very complex setup and bulky optics necessary in instrumentation [7, 14, 21, 22]. On the other hand, using the optical waveguides such as fiber optics in the SPR biosensors provide numerous advantages such as easy to control incident wave guide through the sensor area and simple optic setup. Despite the instrumentational advantages, sensitivity of this device hasn't reached the level of the device with prism based device [23, 24].

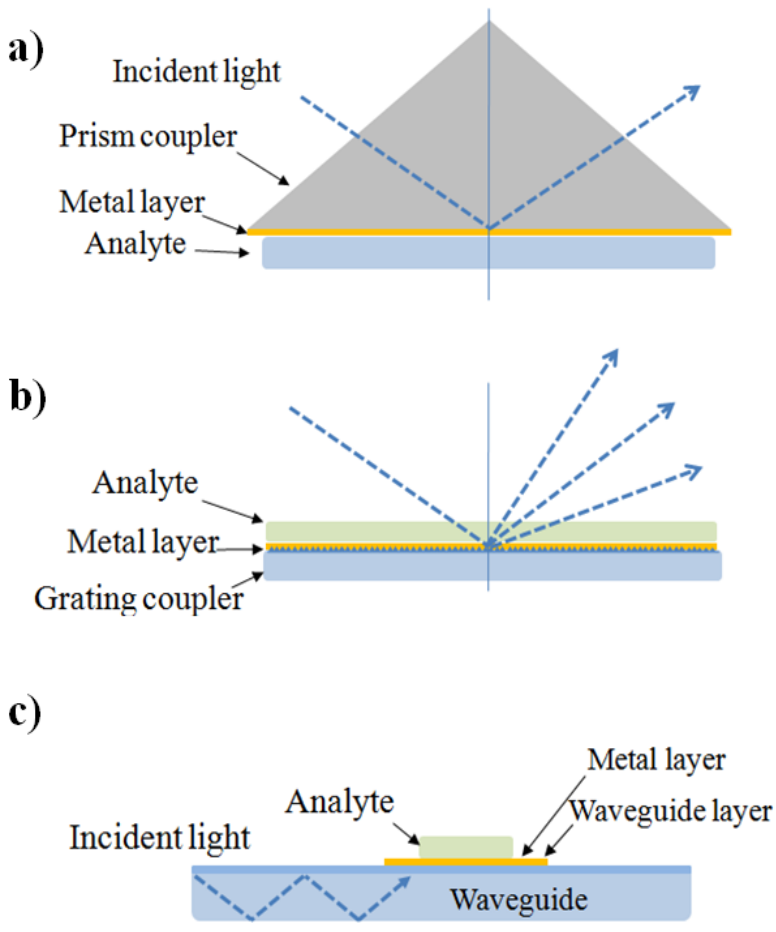

Figure I-1. General configuration of the SPR sensors (a) prism coupler-based SPR system (b) grating coupler-based SPR system (c) waveguide-based system

I.1. Localized surface Plasmon resonance (LSPR) biosensors.

In the past two decade, development of the high sensitive optical biosensors for medical diagnosis such as monitoring of disease, detection of the biological agents and drug discovery has considerably drawn attention of researchers. Sensitivity and capability to detect real-time analysis of bio-molecular interactions allow them to be greatly used in medical diagnosis. The resonance phenomenon of free electron waves in metal nanoparticles (NPs) and nanometer-scale rough surface is called localized surface Plasmon resonance (LSPR) [24, 25]. LSPR excitation produces enhanced local electromagnetic fields near the surface of the metal NP. These electromagnetic fields are highly sensitive for ambient dielectrics as well as the conventional SPR [16, 24, 26]. Figure I-2 shows basic mechanism of the SPR and LSPR. The characteristics of the LSPR biosensors depend on its NP shape, size, inter-particle distance and nature of the material property [16, 27-31]. The most widely used method for LSPR biosensor is the wavelength shift change measurement caused by the local dielectric environment change of the sensor area due to the analyte

adsorption. Scheme I-1 illustrates the most common method for the preparation of the LSPR biosensors [7, 21].

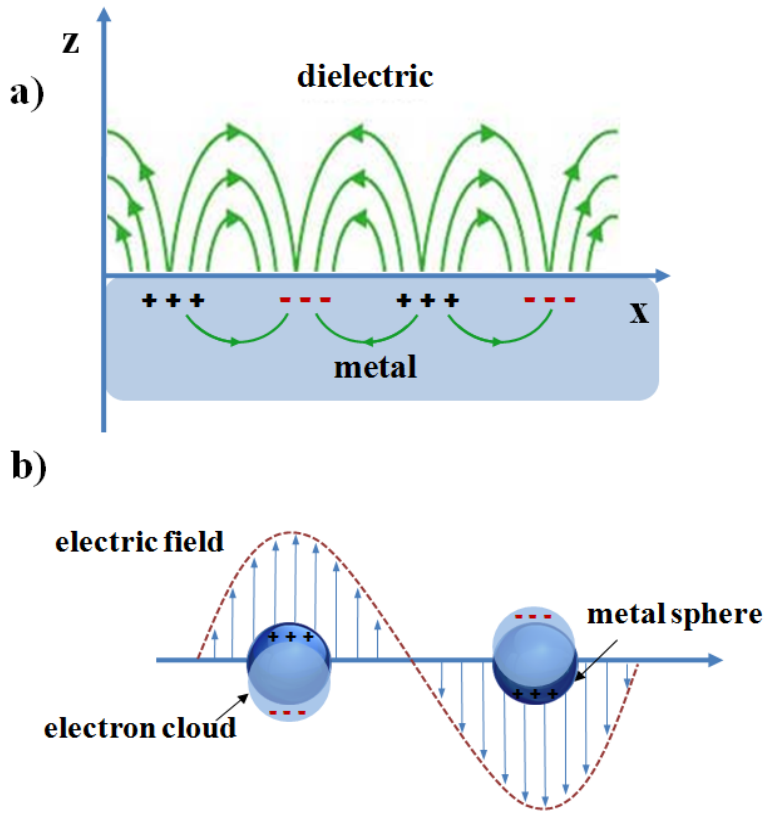

Figure I-2. Basic mechanism of the (a) surface Plasmon resonance and (b) localized surface Plasmon resonance.

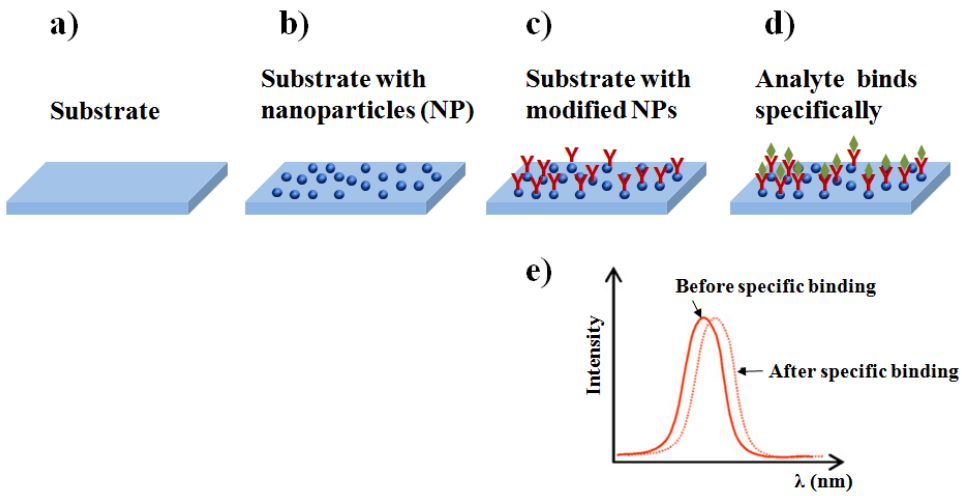

Scheme I-1. General preparation method of the LSPR biosensors based on refractive index changes. (a) Preparation of the substrate. (b) Metal nanoparticles are attached on the substrate using linker chemicals or prepared by nanolithography. (c) Bio-modification of the nanoparticles. (d) Specific binding of analyte such as antibody-antigen reaction. (e) LSPR shift change due to the refractive index change around the nanoparticles.

I.2. Optical geometry for LSPR biosensor

The most common optical geometries that are widely used in LSPR biosensors are transmission [32] , reflection [33], dark-field scattering [6, 31] and total internal reflection (Kretschmann configuration) [7, 15, 34]. Figure 3 illustrates the optical geometries. For instrumentation, both transmission and reflection geometries (Figure I-3 (a), (b)) require simple setup. But the dark field based and prism coupler based LSPR biosensors (Figure I-3 (c), (d)) require complex setup in instrumentation.

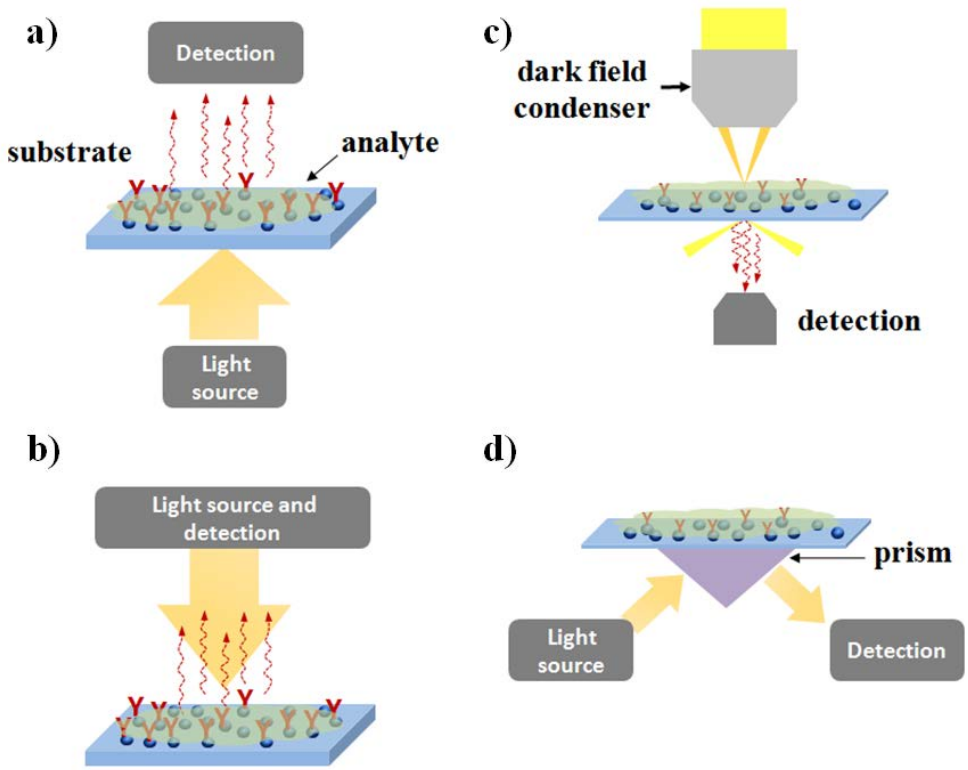

Figure I-3. Widely used optical geometries for LSPR biosensors. (a) Transmission, (b) reflection, (c) dark-field scattering, and (d) prism coupler based setup.

II. Surface enhanced Raman spectroscopy for bio-molecular Detection

Before the discovery of the surface enhanced Raman scattering (SERS), the application of the traditional Raman spectroscopy was limited because of its relatively weak signal.

Fleischmann *et al.* in 1974 first observed intense Raman scattering from aqueous solution of pyridine adsorbed onto silver electrode, which was later identified as an optical phenomenon called surface called surface enhanced Raman scattering (SERS) [35-37]. Since then, SERS research accelerated dramatically until now with contributions from many field of researcher. There are two types of primary theory of the mechanisms of SERS which are the chemical enhancement and electromagnetic enhancement. As yet known, observed enhancement of the Raman signal as high as 10^{14} times and it can be allow detecting single molecule [38-41]. This phenomenon encouraged the researchers to study for various surface enhancement methods and techniques. Currently, SERS spectroscopic technique has become widely used technique for chemical analysis and bio-molecular detection. Main advantages of the SERS compared with other detection methods are the inherent molecular specificity, relatively large sensitivity

and sharp spectral signals [38, 40, 42, 43]. For instance, comparing the fluorescent labels with about 75 nm bandwidth [44] or quantum dots with about 30 nm bandwidth [45] the band width of SERS is as little as few nanometer (*ca*. 1nm) [38, 39]. This relative sharpness of the SERS signal can allow detecting multiple targets without spectral overlap.

III. Fiber optic and its application for bio-detection

Since the development of low-loss fiber optic (FO) the unique features of light guided mode have drawn attention [33, 46]. FO delivers lights with little energy loss to the surroundings due to the total internal reflection (TIR). Depending on the light traveling there are two types of FO: One is single mode and the other is multi-mode. Basic light traveling mechanism through the FO and general structure of the FO is shown in figure I-4 [32, 47]. The FO is generally comprised of a core, cladding and protecting buffer layer (Figure I-4 a) [48, 49].

In early 1970, FOs were first used as chemical sensors, since then the application of the FO spread to many different areas such as environmental, industrial, military, food and biomedical sensors [50-54]. Depending on the bio-receptor component biosensors are classified into five groups which are the enzyme based, antibody, nucleic acid, biometric receptors and cell based [55, 56].

FO biosensors can be used in various types of spectroscopic technique, such as fluorescence, absorption, Raman and as well as SPR spectroscopy.

There are numbers of studies for FO biosensors combined with SPR or SERS spectrometry with different geometry and various types of sensors [57-61]. But there are no reports that measured SPR and SERS simultaneously based on FO. Using FO to measure LSPR and SERS simultaneously instead of prism and it can be used as a portable sensor for real-time chemical and biological detection, because it has the advantages of low cost, simple optical system, and remote sensing.

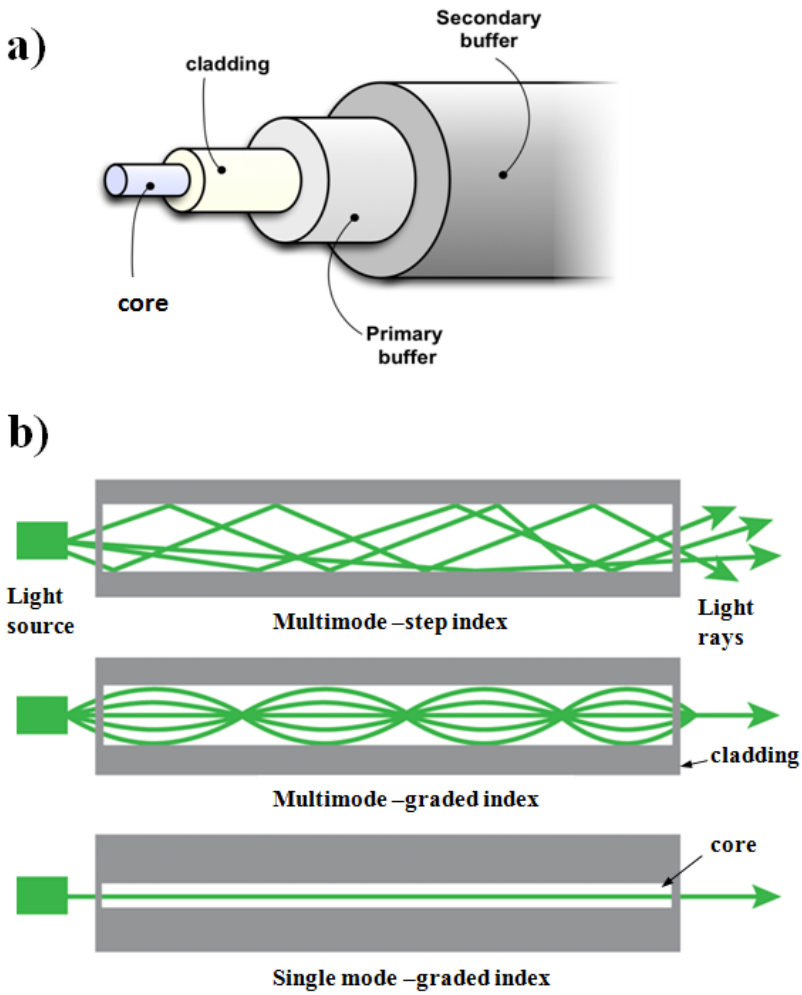

Figure I-4. Fiber optic (FO) structure and light traveling mechanism through the FO. (a) Basic FO structure. FO formed by a core, cladding and protecting buffer layer. Core generally made silica but it can be various materials depending on the purpose of application. (b) The light traveling mechanisms through the FO.

IV. Noble metal nanoparticles for bio-molecular detection

The unique optical and electronic properties of noble metal nanoparticles (NPs), have attracted considerable attention in various fields. In the visible or near infrared region they exhibit distinctive extinction bands due to surface plasmon (SP) oscillation of free electrons [62-65]. These unique optical properties have resulted in extensive application of the nanoparticles as surface-enhanced Raman scattering (SERS) sensors [24, 39, 66], opto-electronic nano-devices [67, 68], photochemical catalysts [69, 70] and biosensors [34, 46, 71-73]. Integrating the noble metal NPs with bio-molecules give a chance to detect various kind of biological process such as bio-imaging, drug delivery, therapy, catalysis and controlling the structure of bio-molecules. In particular, large numbers of study have been done for the silver and gold nanoparticles application for bio-detection. These noble metal NPs based biosensors are summarized in Table I-1 [62].

In most of the noble metal based biosensors, significant parameters such as sensitivity, reliability and reproducibility strongly depend on the particle homogeneity, size, and shape [62, 74-78]. There are various kinds of synthesizing methods. Specially, the most common methods are chemical

reduction, thermal decomposition, vapor deposition and photochemical reduction. But in all synthesizing methods ultimate goals are to obtain NPs with good homogeneity and well controllable shape and size in order to detect bio-molecules better [78-86]. In a variety of practical applications, including surface Plasmon resonance (SPR) and surface enhanced Raman scattering (SERS) sensors for bio-detection, noble metal nanoparticles attached to a glass slide or optical fiber are required for increased sensitivity [27, 87-89]. In addition to sensitivity, reproducibility is important for practical application. In this aspect, in order to fabricate uniform substrates with increased sensitivity and reliability in measurements, e-beam lithography, vacuum sputtering, and wet chemical methods have usually been used for deposition of nanoparticles onto the substrate [1-3, 79, 82, 90]. However, issues such as high cost of e-beam method and morphological non-uniformity of wet chemical methods hindered sensitive and reproducible fabrication of the sensor substrate. Recently, several photochemical reduction methods have been demonstrated to grow silver or gold NPs directly on a glass substrate or FO surface in aqueous solution [62, 89, 91-94].

Method	Type of NP	Target/Samples [reference]
Colomrimetric /scanometric	Gold	• Mutations in EGFR gene in genomic DNA • SNP associated with long QT syndrome in genomic DNA [31] • PCR [43,45] • SNPs in MBL2 gene in genomic DNA—mediated by PCR [53,54]
	Gold	• Melamine in whole milk [40] • Prostate specific antigen (PSA) in human serum [63] • Mutations associated to methicillin resistance in S. aureus & Factor V Leiden mutants [58]
	Gold/silver alloy	• TP53 gene [28] • BCR-ABL fusion genes [29]
NIR	Gold	• Prostate cancer cells in mouse [74] • Lymph nodes in mouse [76] • Brain vessels in mouse [77–79] • HER2 cancer biomarker in breast adenocarcinoma cells [80,81]
SERS	Gold	• Multiple pathogen DNA in clinical specimens (cerebrospinal fluid, stool, pus, and sputum) [118] • Feline calicivirus (FCV) antibody from cell culture media [105] • Prostate-specific antigen in human serum • Deep-tissue imaging in living mouse [123]
	Silver	• HIV-1 DNA in genomic DNA - PCR mediated [112] • Glucose in rat [93]
	Gold silver /core shell	• Phospholipase Cγ1 biomarker protein in cancer cells [122]
Fluorescence	Gold	• Plasmodium falciparum heat shock protein in infected blood cultures [135]
	Silver	• miRNA-486 expression levels in lung cancer cells [145] • Cell membrane imaging in cell lines [146,147]

Table I-1. Summary of the noble metal NPs based biosensors detection

(Cited from reference: [62])

V. Photo chemical method of the noble metal nanoparticles synthesize and growing

Photochemical reduction method has additional merits compared to the wet chemical method, such as improved adhesivity on surface while achieving simple and cost-effective fabrication [74, 91, 92, 95, 96]. The reaction mechanism of the photo-reduced synthesis has not yet clearly understood. But briefly, by the photo-activation different size and shape of metal NPs are formed in the solution or directly grown on the substrate surface [64, 74, 93, 94, 97-101]. Scheme I-2 shows basic mechanism of the photo-reduced synthesis. Scheme I-2 (a) illustrates a synthesizing mechanism of the metal NPs in solution phase. Many groups working on photo-reduced synthesis and main goal of these groups concerned on to obtain methods that make a homogeneous well shape controllable noble NPs. Depending on the parameters such as reducing agents, various incident light sources and its power, and illumination time the NPs can be synthesized with different shape and sizes such as spherical [94, 95], wire [100, 102], triangle [94, 103] and core shell structure [96]. More recently, Ravula et al. reported that silver or gold nanoparticles and alloyed silver and

gold bimetallic nanoparticle decorated aminoclays had been synthesized via the photochemical method in water at room temperature [104].

As well as, the metal NPs can be directly grown on the substrate and the mechanism is shown in scheme I-2 (b). Substrate can be various types such as glass or FO etc. For instance, Canamares et al. had grown silver nanoparticles on glass substrates [92], Y. Niidome et al. reported dodecanethiol-passivated gold particles grown on glass substrates using 532 nm laser radiation [93, 103], R.Lombardi's group developed silica cored FO silver SERS chemical sensors by photo-induced growing [101]. All these groups mentioned that photo chemical method is the significant studying object of the NPs synthesize and it has the unique advantages such as cost effective, saving time and so on. Many of the practical applications, such as surface Plasmon resonance (SPR) and surface enhanced scattering (SERS) sensors for bio-detection, noble metal nanoparticles attached to a glass slide or optical fiber. E-beam lithography, vacuum sputtering, and wet chemical methods have usually been used for deposition of nanoparticles onto the substrate. Increasing the sensitivity, reproducibility and reliability of the sensors are significantly necessary. However, high cost of e-beam method and morphological nonuniformity of wet chemical methods hindered sensitive and reproducible fabrication of the sensor substrate. Currently,

preparing the substrates or sensors with easily and cost effectively plays one of the significant roles in photo-reduced growing.

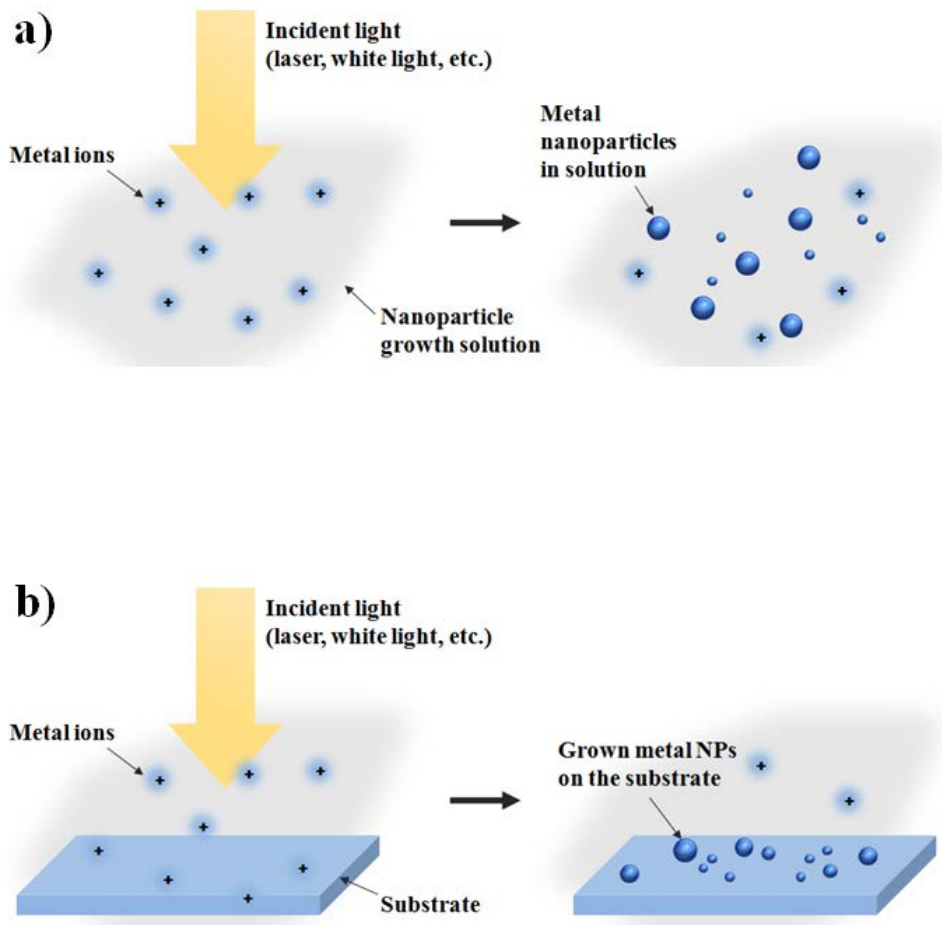

Scheme I-2. Basic mechanism of the photo reduced synthesis. (a) Metal NPs are formed in solution phase. Incident light source can be laser or white light such as a Xenon lamp. (b) Metal NPs are directly grown on the substrate. Substrate can be various types such as glass or FO etc.

VI. Research Objective

LSPR is a label free and non-specific technique because the resonance signals dependent on the refractive index around the metal NPs on the substrate, and the specificity of bio-molecular reaction is only obtained from identification biomaterials such as antibodies. Combining of the LSPR spectroscopy as a binding monitoring tool with SERS spectrometry as a recognition tool, can widen the range of applications, allow differentiating the analyte and improvement of the detection limits, especially for bio-molecular reaction. While LSPR can measure real-time binding process of the bio-molecular reaction quantitatively, SERS signal will distinguish the type of analytes binding or absorbing to the sensor. There are few reports that measured SPR and SERS simultaneously [105-109]. General design of these setups based on Kretschmann's configuration and need very complex setups. On the other hand, capability of bidirectional propagation of the light through the FO gives a possibility to detect multiple signals from the analytes in one time easily. Using FO it is possible to measure LSPR and SERS simultaneously instead of prism and can be used as a portable sensor for real-time chemical and biological detection, because it has the advantages of low cost, simple optical system, and remote sensing.

Therefore, one of the research objects of this study was to innovate unique FO biosensor based LSPR and SERS simultaneous detection system and its application for the bio-related detection. The results, LSPR and SERS simultaneous detection system configuration and fabrication of the FO based biosensor were described in Chapter II.

Mono-disperse fabrication of plasmonic nanoparticles on silica substrate such as glass and FO surface is one of important issues for reliable optical sensors utilizing plasmonic properties such as LSPR and SERS. Even though there have been many approaches such as e-beam lithography, vacuum sputtering, and wet chemical methods that have usually been used for deposition of nanoparticles onto the substrate. However, issues such as cost of e-beam method and morphological non-uniformity of wet chemical methods hindered sensitive and reproducible fabrication of the sensor substrate. Photo reduction method can solve these problems easily and cost effectively. Several photo-induced methods have been demonstrated to grow silver or gold nanoparticles directly on a glass substrate or FO surface from their aqueous solution. But the morphologies of the photo-induced grown NPs on the substrate have not reached enough uniformity.

Sensor improvement method based on photo reduction was described in Chapter III. By incorporating self-assembled monolayer of amine and non-

amine functionalized silane on a glass substrate, silver nanoparticles (Ag NP) were fabricated highly mono-dispersedly on the substrate by photo reduction in an aqueous solution of silver nitrate and sodium citrate. As criteria of mono-disperse growing, the average diameter of Ag NPs, the degree of monomer, and the surface coverage of Ag NPs were monitored. The ratio of silane coupling reagents with and without amine group, the photo-reduction time and the concentration of growth solution were found to be critical control factors. By controlling these factors mono-disperse and uniform growth of Ag NPs could be obtained.

Chapter II.

Fiber-Optic Sensor Simultaneously Detecting LSPR and SERS

I. Experimental section

I.1. Chemicals and material

Chloroauric acid ($HAuCl_4 \cdot 3H2O$, 99.9%), 3-aminopropyl-dimetylethoxysilan (APMES, 97%), trisodium citrate (99%), 4-aminothiophenol (ATP, 97%), bovine serum albumin (BSA, 10%), phosphate buffered saline (1x PBS, pH 7.4) were all purchased from Sigma Aldrich and hydrogen peroxide (H_2O_2, 30%), sulfuric acid (H_2SO_4, 95%), methanol (99.5%), ethanol (99%) were of analytical grade and were supplied by Daejung Chemicals and borate buffer (10 mM, pH 8.5) were supplied by GE Healthcare and antibody interferon-gamma (Purified Anti-Human IFN-γ), antigen interferon-gamma (Recombinant Human IFN-γ) were purchased from Becton Dickinson. The refractive indices solutions were purchased from Cargille Labs. (Series AAA).Multimodal fiber optic whose core diameter 105 μm and cladding thickness of 20 μm was purchased from Thorlabs (Model: AFS105/125Y).

I.2. Preparation of the fiber optic

First, a 15 cm long fiber optic (FO) was cut and its protecting polymer cover was removed carefully around 4 cm long from both ends of the FO. Then, the both ends were washed with water and acetone and dried under nitrogen 3 times.

Second, both ends of the FO were cleaved to expose a smooth silica surface using optical fiber cleaver (FITEL S325, Furukawa Electric) and the surface smoothness was checked using a fusion splicer. Then, one end-face of the FO was activated with hydroxyl functional groups by dipping into the piranha solution (H_2SO_4 : H_2O_2; 4:1) for 20 min at 95ºC for preparation of further silanization. Figure II-1 shows the FO after piranha activation and laser propagation through the FO.

a)

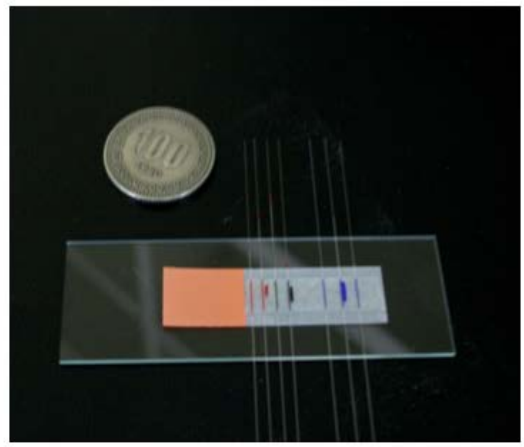

b)

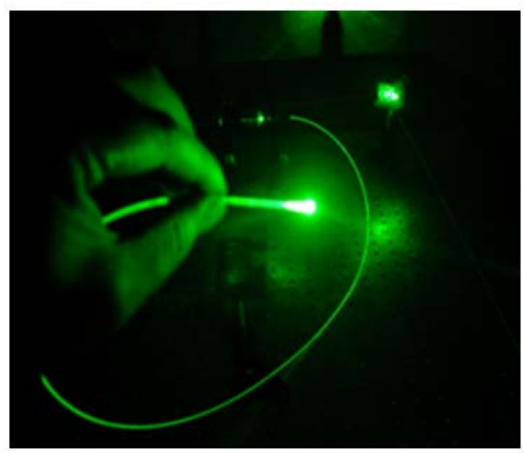

Figure II-1. FO after piranha activation (a) and laser propagation through the FO (b).

I.3. Preparation of gold nanoparticle

The gold nanoparticles (Au NPs) were synthesized by reduction of chloroauric acid [57, 58, 110]. Fifty milliliter of 0.01% (w/v) $HAuCl_4$ aqueous solution was boiled in oil bath at 100 º C and 0.5 ml of 1% (w/v) trisodium citrate aqueous solution was added in a 0.01% (w/v) $HAuCl_4$ solution during the heating. After the solution was boiled with vigorous stirring for 20 minutes, the color of the solution was changed from bright yellow to red. Scanning electron microscope (SEM), DF microscope and UV adsorption microscope were used to characterize particle size and the average diameters of the Au NPs were estimated to be about 50 nm. In this method, the less amount of sodium citrate was added, the larger diameter of Au NPs was obtained. SEM and DF images are shown in Figure II-2 (a), (b). Extinction and scattering spectra of the Au NPs are shown as Figure II-2 (c). Extinction spectrum was measured with a commercial UV-Visible adsorption spectrometer and scattering spectrum was measured with a homemade DF system.

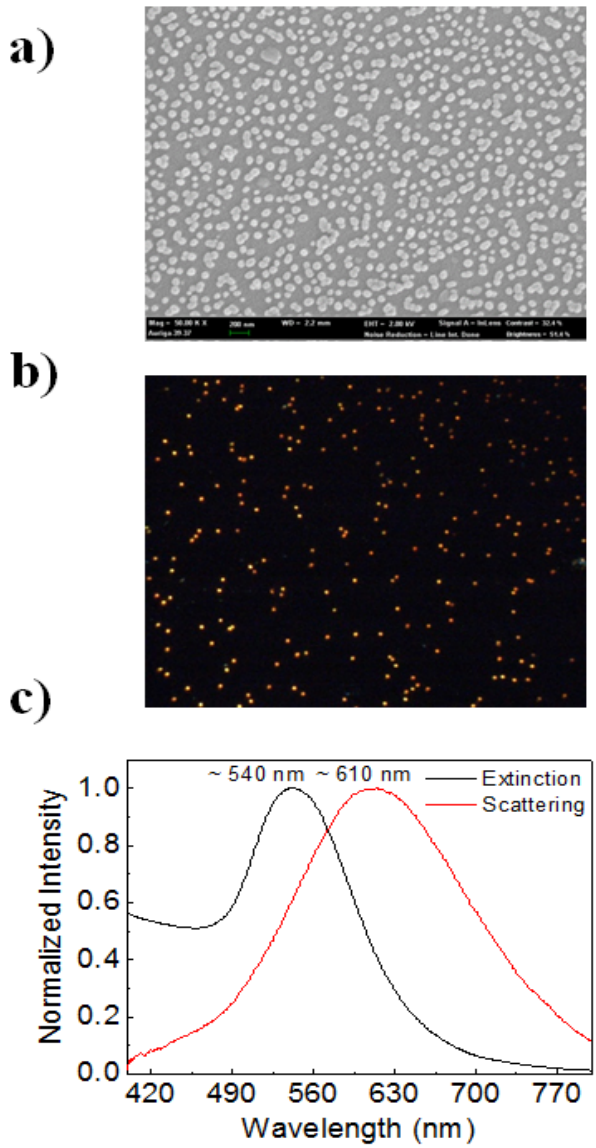

Figure II-2. Characteristics of the Au NP after preparation. (a) SEM image. (b) DF image. (c) Extinction and scattering spectrum. Extinction spectrum was measured with a commercial UV-Visible adsorption spectrometer and scattering spectrum was measured with a homemade DF system.

I.4. Fabrication of the fiber optic LSPR and SERS sensor probe

In order to fabricate the FO LSPR and SERS sensor, Au NPs should be formed on the end-face of the optical fiber. Therefore, FO with activated hydroxyl functional groups was then immersed into 5% (v/v) APMES solution for 90 min to form a self-assembled monolayer (SAM) on the end-face of the FO. Next, the FO was immersed into gold colloid solution during 60 min for immobilization of the gold nanoparticles on the FO end-face. The FO sensor probe surface was then characterized by field emission scanning electron microscope (Carl Zeiss, SUPRA 55VP). Figure II-3 shows SEM image of the FO sensor probe. The end-face of the FO sensor probe shown in Figure II-3 (a) and the Figure II-3 (b) is the zoomed-in image. The diameter of the gold nanoparticles were founded approximately 50±5 nm in average.

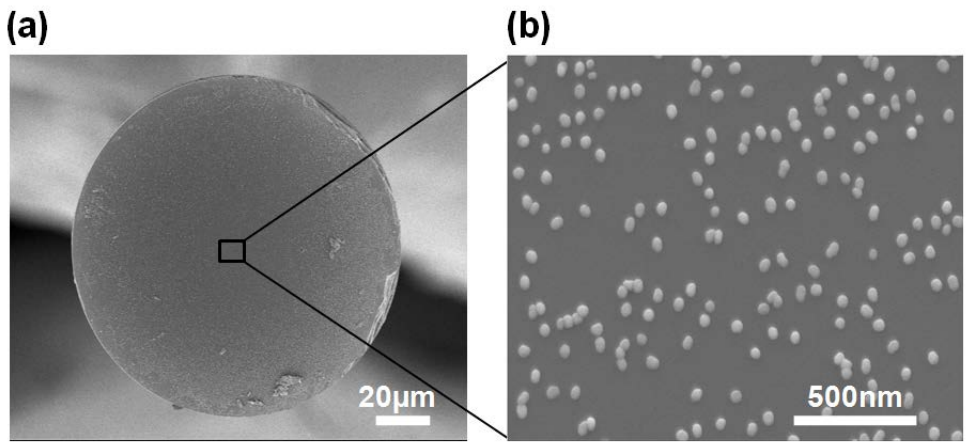

Figure II-3. SEM image of the FO bio-sensor probe after Au NPs immobilization. (a) End-face of the FO sensor probe and (b) is the zoomed-in image. Average diameter of the Au NPs were founded approximately 50±5 nm in average.

I.5. Fabrication of the FO LSPR and SERS sensor for label-free immunoassay

In order to investigate the possibility of detecting a bio-molecular reaction, the sensor was used to detect antibody-antigen reaction of IFN-γ. For this purpose, Au NPs immobilized FO sensor probe was further immobilized with antibody of IFN-γ.

First, 4-aminothiophenol (ATP) was used as Raman reporter molecule and the FO sensor was immersed in 100 µl, 10^{-3} M ATP ethanol solution for 3 hours. In this process, the molecules ATP conjugated to the surface of the gold nanoparticles on the end face of the FO sensor. FO sensor was then immersed into 100 µl, 20 µg/ml antibody IFN-γ borate buffer (pH 8.5) solution for 15 min. Herein, the antibody IFN-γ was mostly immobilized on gold nanoparticles on the surface of the FO sensor, because the Au NPs have negative charges on their surface. On the other hand, the amino-functional groups of the SAM, which are formed at the end-face of the sensor, make positive charges on its surface. Therefore, the binding force of the Au NPs with the antibody is stronger than that of the SAM on the surface of the sensor.

Finally, the FO sensor is treated with Bovine Serum Albumin (BSA) in order to protect nonspecific binding. The FO sensor was immersed into 100 μl of 1% BSA borate buffer (pH 8.5) solution for 15 min. The BSA was adsorbed on the whole surface of the sensor, except for antibody IFN-γ, and will protect the binding of antigen IFN-γ to the surface of the sensor, except for antibody IFN-γ. In order to confirm the immobilization process of the APT, antibody and BSA, we measured the SPR signal during its overall process. Scheme II-1 illustrates immobilization process of antibody IFN-γ on the FO LSPR and SERS sensor surface.

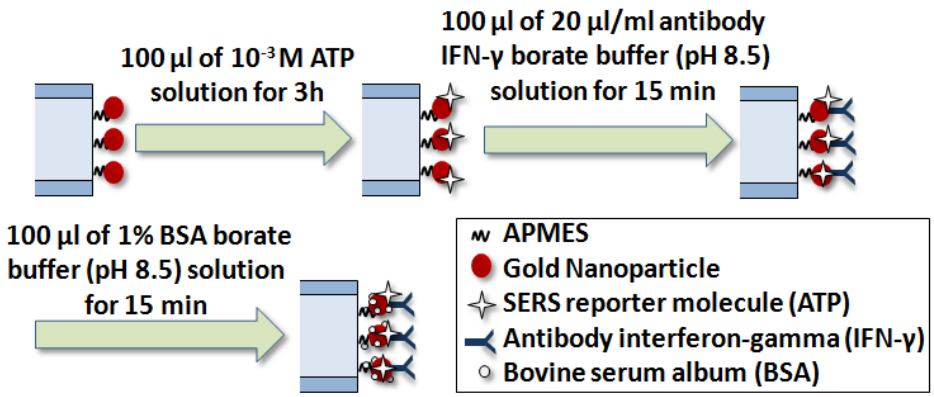

Scheme II-1. Antibody IFN-γ immobilization process on the FO LSPR and SERS sensor substrate.

I.6. Assembling of Dark Field and SERS, Fiber Optic LSPR and SERS Simultaneous detection system

Scheme II-2 shows the main concept of the FO LSPR and SERS simultaneously measuring system. The system consists of two parts. One part is for detection of SERS and another is for detection of LSPR. Simply, light is delivered and focused get in through in FO from its one end via some optics and filters until to the opposite end which has the sensor area. Using the edge filter SERS signals can be detect and using beamsplitter LSPR signals can be detect from back reflected direction of the FO. Scheme II-3 shows the light traveling mechanism through the FO LSPR and SERS sensor probe. The smooth line shows light into the FO sensor and dashed line shows the scattered signal from the FO sensor.

Scheme II-4 shows DF and SERS, FO LSPR and SERS simultaneous detection system which we were used to study this research. Basically, in case (a) this system detects DF images, scattering spectrum and SERS signals. In case (b), the system detects FO LSPR and SERS.

Two light sources were used which are the tungsten-halogen lamp (Nikon, LHS-H100P-1) for DF image, scattering spectrum and tunable Ar-

Kr ion laser (Melles Griot, 35-KAP) for SERS and LSPR. The laser center wavelength was 647 nm and laser line filter (Lambda Research Optics, 647.1-F10-25.4) was used to remove multi-lines of the laser. Nikon microscopy (Eclipse, TE2000-s) was used and additionally assembled with DF condenser (Nikon, T-CHA, oil 1.43-1.20) upper side of microscopy and ×100 oil type objective lens (Nikon, Plan Flour, WD = 0.16, 0.5-1.3 NA oil, iris) was in bottom side.

In case (a), left side of the microscopy DF images and scattering spectrum detects. Scattered lights from the sample collected by ×100 oil type objective lens and delivered to flip mirror and CCD #1 (Nikon, DS-Fi1) detected DF images with right angle. Photomultiplier tube (Acton Research, PD-471) was assembled with monochromator (DongWoo Optron, DM-151i) and operating program was written in LABVIEW and calibrated. Opening the flip mirror, this small system detects scattering spectrum.

For SERS measurement, laser light (647 nm) delivered to the sample from the behind of the microscopy via line filter (Lambda Research Optics, 647.1-F10-25.4), wave plate (Sigma Koki, WPM-30-2P), cubic beam splitter (Thorlabs, PBS051), beam expander (Thorlabs, BEP32), mirror and edge filter #1 (Lambda Research Optics, LWP-2502B-650, cut-on wavelength = 650 nm). Back reflected direction from the sample, which

means behind the microscopy SERS signals detected via CCD #2 (Andor DU401, -70°C) equipped with a spectrometer (Horiba Jobin Yvon Triax-320).

In case (b), laser light (647 nm) delivered to the FO sensor via line filter, wave plate, cubic beam splitter and edge filter #2. 10x objective lens (Olympus, 0.25 NA, WD=10.6 mm) was used to collect the laser into the FO sensor. From the edge filter #2, the back scattered signal separates two directions which is the transmitted one for the SERS and reflected one for the LSPR detection. SERS signal measured by CCD #2 (Andor DU401, -70°C) equipped with a spectrometer (Horiba Jobin Yvon Triax-320). LSPR peak shift change was measured as intensity profile of 647 nm laser and it was detected digital power meter (Thorlabs, PM100D) with the photodiode power sensor (Thorlabs, S121C). Figure II-4 shows real image of the DF and SERS, FO LSPR and SERS system.

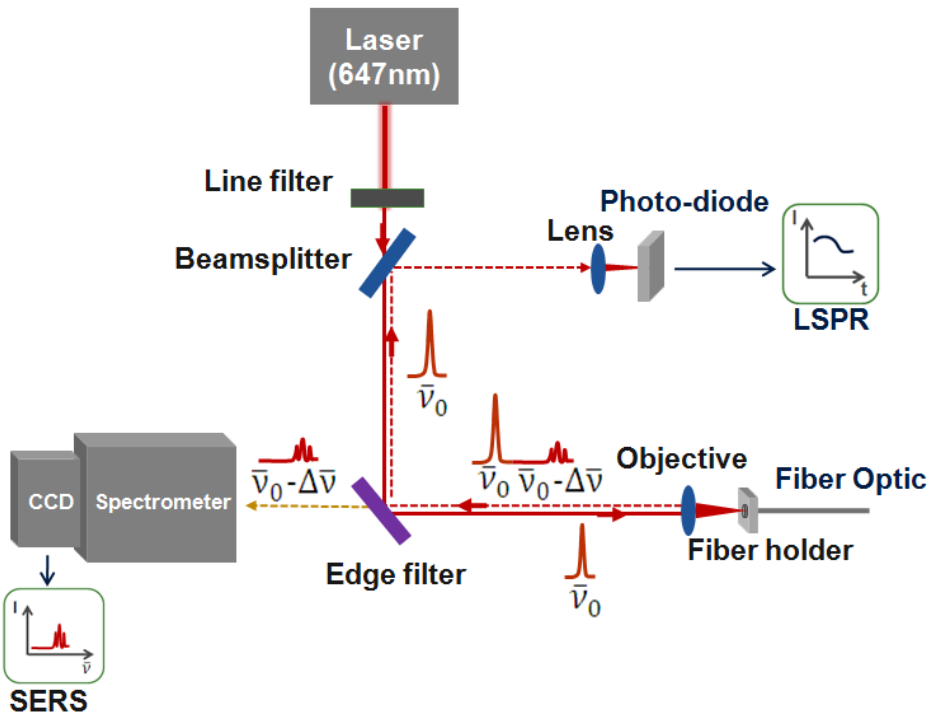

Scheme II-2. Main concept of the FO LSPR and SERS simultaneously measuring system. Incident laser light (647 nm) was coupled through the FO and back scattered signal from the FO was collected and delivered to edge filter. From the edge filter SERS signal is transmitted and detected by a CCD detector and reflected LSPR signal detected by a photo-diode.

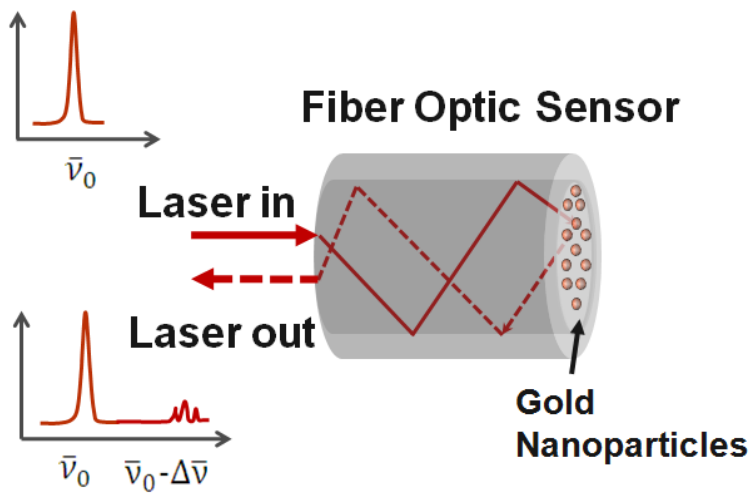

Scheme II-3. The light traveling mechanism through the FO LSPR and SERS sensor. The smooth line shows collimated light into the FO sensor and dashed line shows the back scattered signal from the FO sensor.

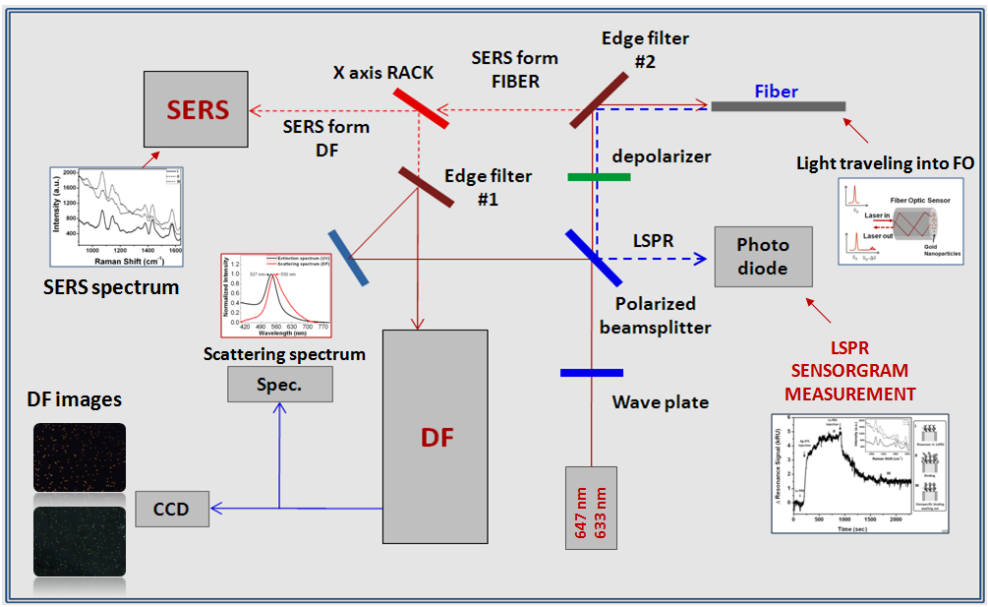

Scheme II-4. A schematic diagram of the Dark Field and SERS, FO LSPR and SERS simultaneous detection system. On the left side of the microscopy (Nikon, Eclipse, TE2000-s) DF images, scattering spectrum detect. Right and behind of the microscopy LSPR and SERS detect respectively. Two light sources were used which are the tungsten-halogen lamp (Nikon, LHS-H100P-1) for DF image, scattering spectrum and tunable Ar-Kr ion laser (Melles Griot, 35-KAP) for SERS and LSPR.

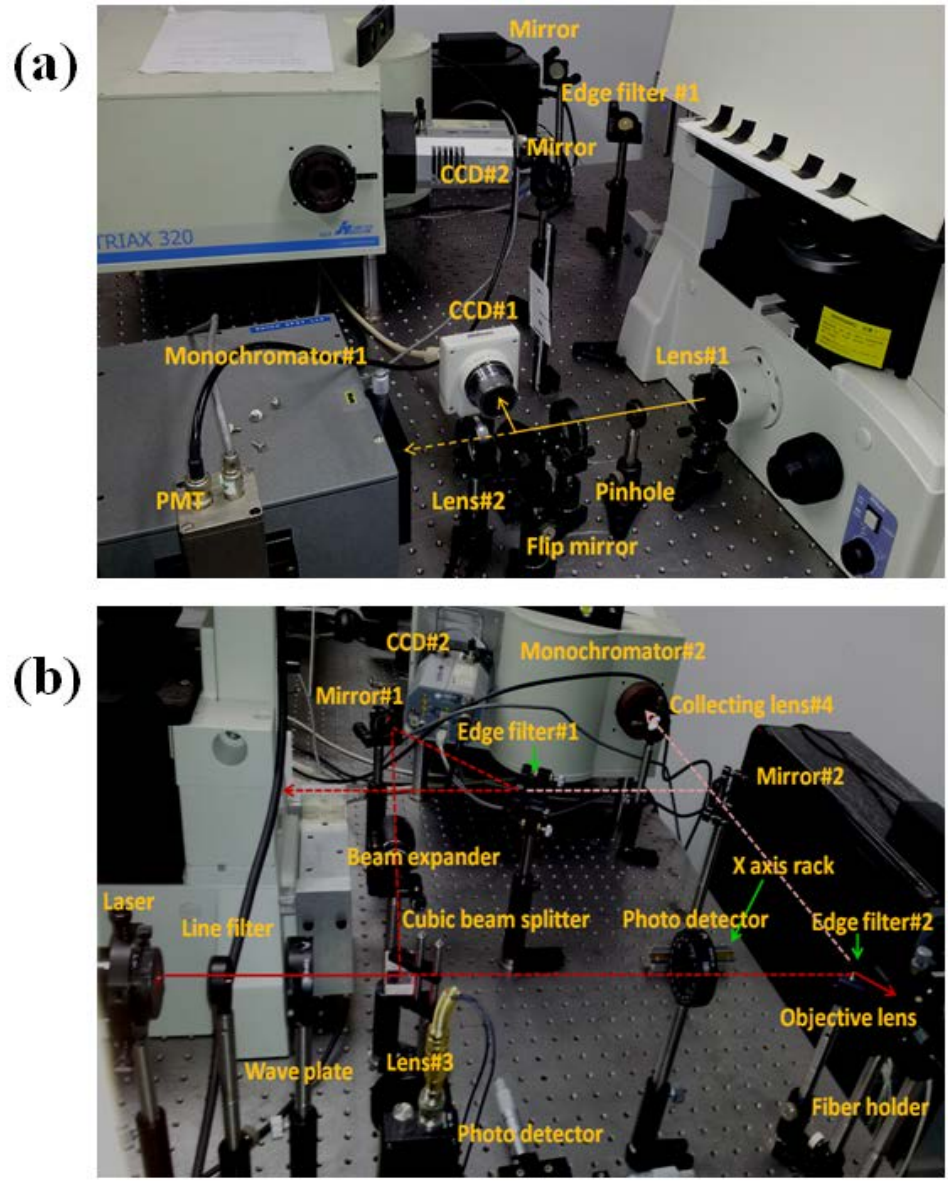

Figure II-4. Real image of the Dark Field and SERS, FO LSPR and SERS simultaneous detection system. (a) shows left side of the microscopy (Nikon Eclipse, TE2000-s) which is the dark field images and scattering spectrum monitoring part. (b) is the right and behind side of the microscopy which is the SERS and LSPR detection part.

II. Results and discussion

II.1. Simultaneous measurements and fiber optic sensor sensitivity

In order to make simultaneous measurements ATP was used as SERS reporter molecule and for checking the FO sensor LSPR sensitivity five different refractive indices solutions (Series AAA, Cargille Labs) were used as sensing medium of which refractive index varies from 1.34 to 1.38. To attach the reporter molecule on sensor surface, FO sensor was immersed into the 10^{-3}M ATP ethanol solution for 3h and rinsed with absolute ethanol and deionizied water (DI) and gently dried with air.

The FO sensor was then first measured in deionized water (DI) of which refractive index was 1.33 as a reference by immersing FO into the DI. Then, it was measured in different refractive indices solutions. Between the measurements FO sensor was washed with ethanol, DI and dried with air. The sample power was 15mW and for the SERS measurement CCD acquisition time was 5 second and for LSPR photo-diode recording time was 5 second with 0.2 second interval.

Figure II-5 shows FO sensor average light intensity change at wavelength 647 nm with various refractive indices solutions. Upper inset shows peak shift change of the FO sensor with refractive index. Tungsten-halogen lamp was used as light source. Bottom inset shows FO sensor real-time measurement of the light intensity change at wavelength 647 nm with various refractive indices solutions. Figure II-6 shows the result simultaneously measured 4-ATP SERS spectrum of the FO sensor with different refractive indices solutions. As the refractive index of the solution increased, intensities of the SERS signals were also increased. Otherwise, the shape of the SERS signal has no big change.

The sensitivity of the LSPR sensor is usually expressed using the intensity modulation, which measures change of the reflected light intensity (ΔI) per unit change of the refractive index (Δn) and expressed as $S=\Delta I/\Delta n$ RIU^{-1} as a function of normalized intensity. For comparison of the performances of various sensors, the measured intensity is normalized and has a dimensionless unit. The normalized intensities mean the relative change of intensities for the reference refractive index as 1.33, so they have dimensionless unit [57, 58, 110]. Herein, RIU means refractive index unit, and the normalized intensity is the relative intensity for 1.33 of refractive

index as a reference. The sensitivity of the FO sensor was determined 13.107 RIU^{-1}.

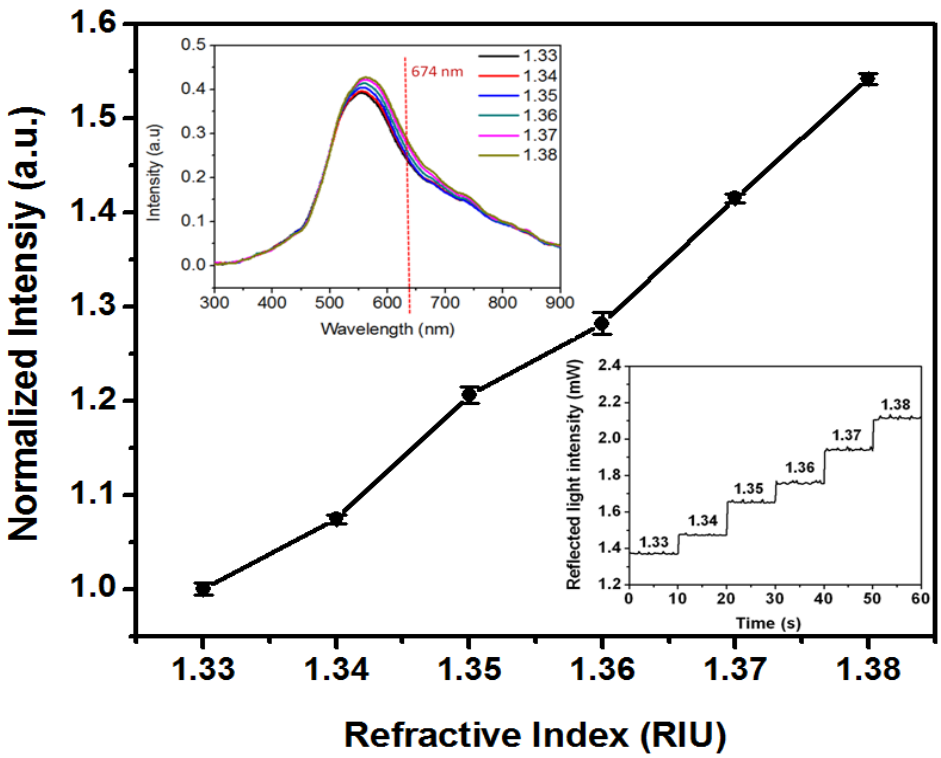

Figure II-5. FO sensor average light intensity change at wavelength 647 nm with various refractive indices solutions. Upper inset shows peak shift change of the FO sensor with refractive index change. Tungsten-halogen lamp was used as light source. Bottom inset shows FO sensor real-time measurement of the light intensity change at wavelength 647 nm with various refractive indices solutions.

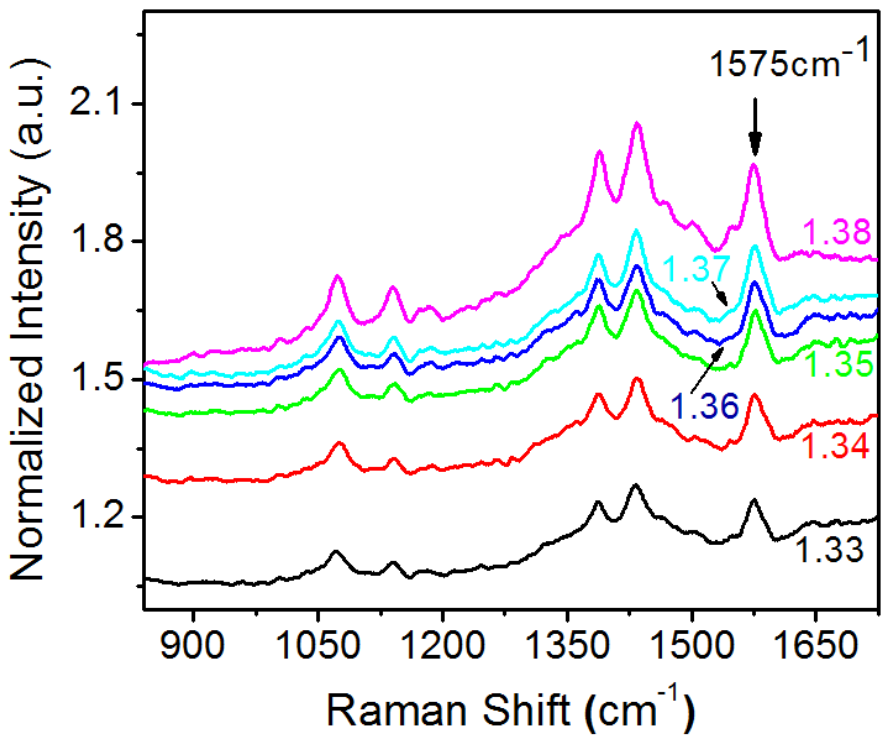

Figure II-6. Simultaneously measured 4-ATP SERS spectrum of the FO sensor in different refractive indices solutions. As the refractive index of the solution increased, intensities of the SERS signals were also increased. Otherwise, the shape of the SERS signal has no big change.

II.2. Real-time sensorgram

To confirm the immobilization process of the APT, antibody of IFN-γ and BSA on the FO LSPR and SERS sensor surface, real-time measurement of the resonance signal was made during its overall process.

Figure II-7 shows LSPR and SERS simultaneous measurement during antibody IFN-γ immobilization on the FO sensor. Figure II-7(a) shows real time sensorgram of the resonance intensity at wavelength 647 nm during the ATP, antibody IFN-γ and BSA immobilization of the FO sensor. It was composed of four steps shown as I, II, III, and IV. FO sensor was used to measure SPR intensity in phosphate buffered saline (1x PBS, pH 7.4) as a baseline and it corresponds to I step. After ATP, antibody IFN-γ and BSA were immobilized on the FO sensor the resonance intensities were also measured in the same condition of the baseline measurement and it correspond to II, III and IV steps respectively. The measured intensity in 1× PBS using the FO without Au NPs was used as a reference and this value was subtracted from the measured intensity at each steps. Due to the comparison, FO without Au NPs was measured same measurements as the FO sensor and it is shown as a gray line in Figure II-7(a). At all steps, this value is almost the same with the intensity measured in 1× PBS, which is

not immobilization of the antibody IFN-γ and BSA due to the absence of the Au NPs on the FO sensor end-face.

The unit of LSPR intensity in the measurement of INF-γ reaction is converted from RIU(Refractive Index Unit) to RU(Resonance Unit) using the reference by Biacore, in which 0.001 RIU corresponds to 1000 RU. The meaning of RIU denotes ΔI/S here ΔI is maximum reflected light intensity difference and S is the sensitivity of the FO sensor probe.

Figure II-7(b) shows ATP SERS spectral changes during the immobilization process of the ATP, antibody IFN-γ and BSA. Dashed, dot-dashed, doted and solid lines correspond to I, II, III and IV steps, respectively. ATP SERS signal's shape and intensity was changed due to the immobilization of the antibody IFN-γ and BSA on the FO LSPR and SERS sensor.

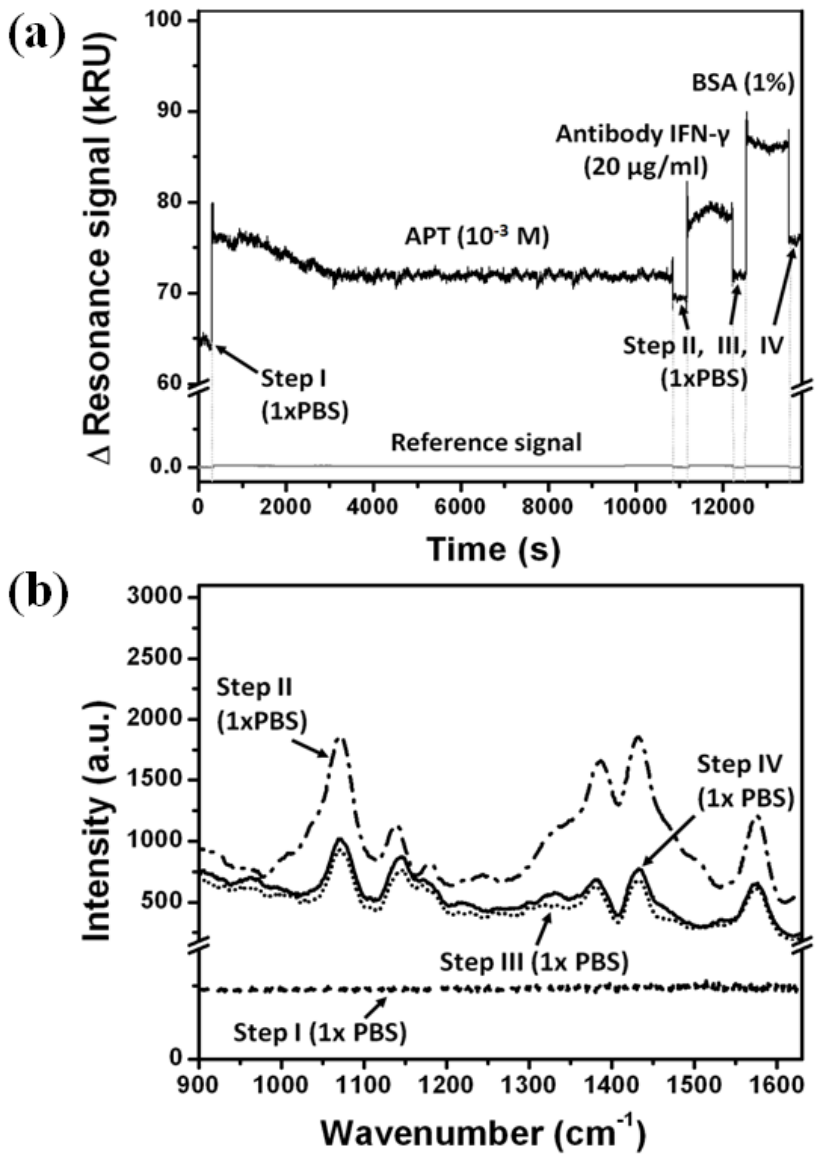

Figure II-7. LSPR and SERS simultaneous measurement during antibody IFN-γ immobilization. (a) Real time sensorgram of the resonance intensity at wavelength 647 nm during the ATP, antibody IFN-γ and BSA immobilization. (b) Simultaneous measured ATP SERS spectrum changes during the immobilization process.

II.3. Real-time detection of antibody antigen reaction of IFN-γ

The real-time simultaneous measurement of LSPR and SERS during the antibody-antigen reaction of IFN-γ was composed of three-step processes as shown in Figure II-8.

Figure II-8(a) shows real time sensorgram of the resonance intensity at wavelength 647 nm. Before the injecting the antigen of IFN-γ, the FO sensor probe was immersed to the 100 μl, 1x PBS during 3 min. The result was adjusted to the resonance signal of 0 kRU as a baseline. The unit of LSPR intensity in the measurement of INF-γ reaction is converted from RIU to RU (Resonance Unit) using the reference by Biacore, in which 0.001 RIU corresponds to 1000 RU. Next, 10 ng/ml antigen IFN-γ was injected and resonance signal was recorded during 12min. Once starting the injection of antigen, the resonance signal increased drastically and then remained constant and average resonance intensity was 4.573 ± 0.13 kRU. The FO sensor probe was then started to inject 1x PBS (pH 7.4) for removing nonspecific binding of antigen of IFN-γ. Resonance intensity was recorded during 24 min until the signal was stabilized. The average resonance signal

change was 1.489 ± 0.11 kRU. Figure II-8(b) shows FO LSPR and SERS sensor surface morphology during the antibody-antigen reaction of IFN-γ.

Figure II-8(c) illustrates the SERS signal changes during the reaction of antibody-antigen of IFN-γ. The dashed, doted and solid lines are belonging to first, second and third steps respectively. The shape of the ATP SERS signal was changed in second step due to the influence from the antibody-antigen specific and nonspecific binding. In the third step the shape of the SERS signal was became almost similar with step one but more intense which means only the specific bound of antibody-antigen of IFN-γ was on the FO sensor and the nonspecific binding was washed out.

One of the major advantages in label-free assays, a property of the target antigen molecule itself is detected. It is very simple because they require only a single capture antibody and provide direct detection. This allows analyzing real-time antibody and antigen binding process. During the binding of antibody to antigen LSPR real time sensorgram was quantitatively detected the binding process on the FO sensor and the other hand SERS was detected qualitatively whether target antigen was bound.

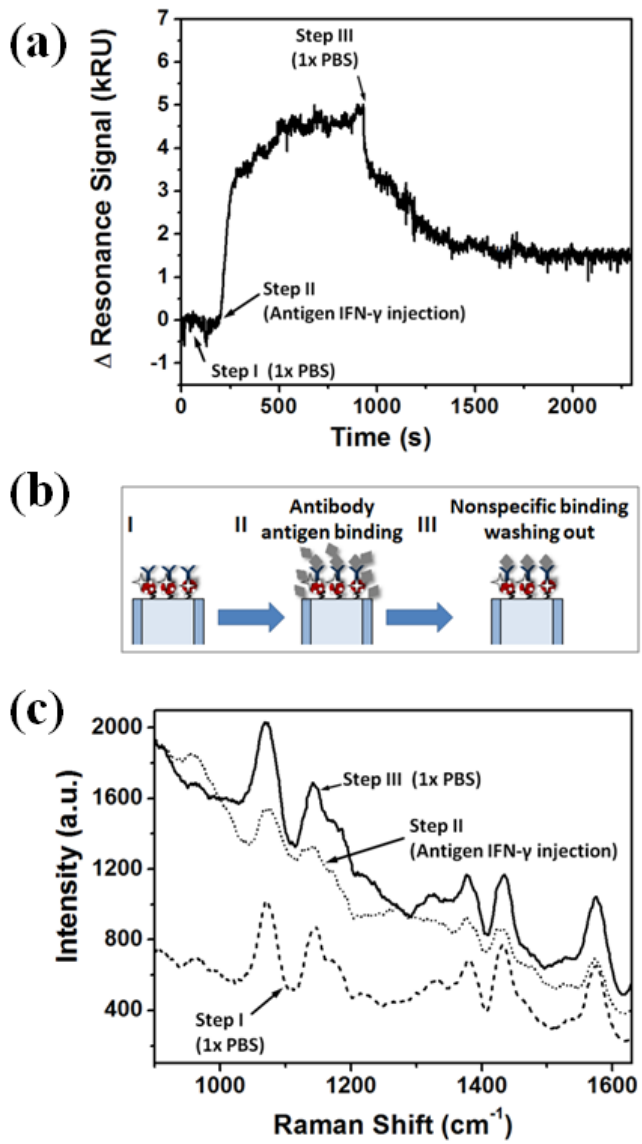

Figure II-8. Simultaneous measurements of the LSPR and SERS during the antibody-antigen reaction of IFN-γ. (a) Real time sensorgram of the resonance intensity at wavelength 647nm. (b) FO LSPR and SERS sensor surface morphology during the antibody-antigen reaction of IFN-γ. (c) Simultaneously measured ATP SERS spectrum during the antibody-antigen reaction of IFN-γ.

Chapter III.

Mono-disperse Growth Control of Silver Nanoparticles on Glass Substrate using Photo-reduction and Mixed Self-assembly

I. Experimental section

I.1. Chemicals and material

Silver nitrate ($AgNO_3$, 99.5%), trisodium citrate (99%), 3-amino-propyldimetylethoxysilane (APMES, 97%) and methoxytrimethylsilane (TMS, 99%) were purchased from Sigma Aldrich. Hydrogen peroxide (H_2O_2, 30%), sulfuric acid (H_2SO_4, 95%), isopropyl alcohol (99.5%), acetone (99.5%) and ethanol (99%) were obtained from Daejung Chemicals. All chemicals used were analytical grade and were used without further purification. Microscope cover glasses (MARIENFELD, 2.4 cm × 4.0 cm) were used as the nanoparticle growing substrate.

I.2. Instrumentations

I.2.1. Photo reduction system

Figure III-2 shows photo-reduction system used in our study. (a) Real image of the system. (b) Schematic diagram of photo-reduction process. The white light employed for photo-reduction experiments was a Xenon lamp purchased from ABET Technologies (ABET Technologies, LS-150-Xe). The light was focused on a glass substrate immersed in silver growing solution. The diameter of the focused beam is *ca*. 4mm. The light power was *ca*. 500 mW measured at 500 nm. Emission spectrum of the Xenon lamp is shown in Figure III-1. In our experiments, we used normal glass container. Therefore, the wavelengths in UV region might be filtered out. However, as shown in the whole spectrum, the difference between Xenon lamp, through glass, and through glass with water is mainly intensity difference rather than spectral difference having sharp and intense peaks between 650 nm to 1100 nm wavelength range. Further study on color effect of silver growing is very important, however, in this study we didn't include this point leaving as next study of this project.

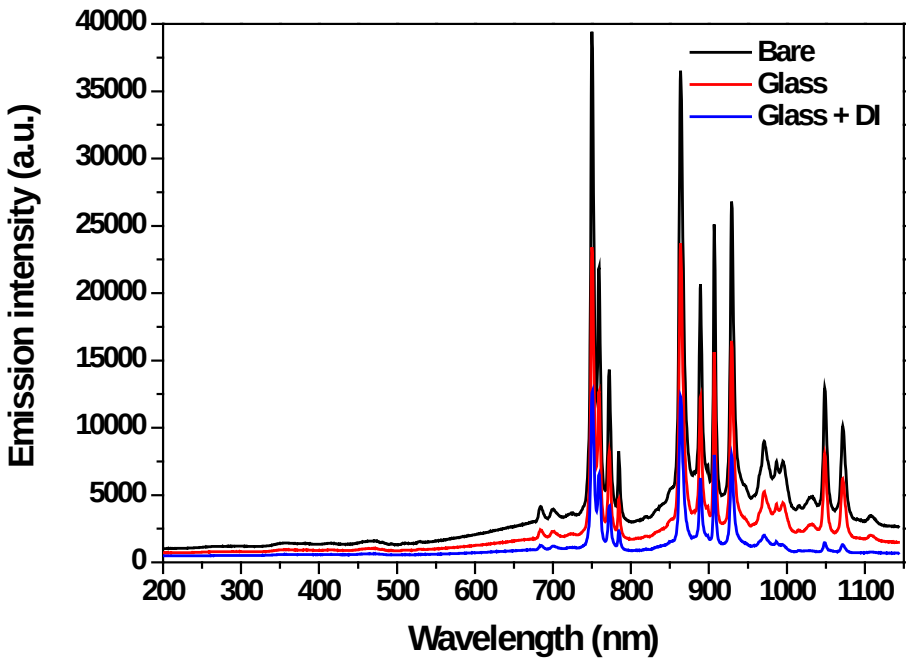

Figure III-1. Emission spectra of the Xenon lamp. Black line exhibits extinction spectrum of the white light. Red and blue lines are light through glass container and glass container plus distilled water respectively.

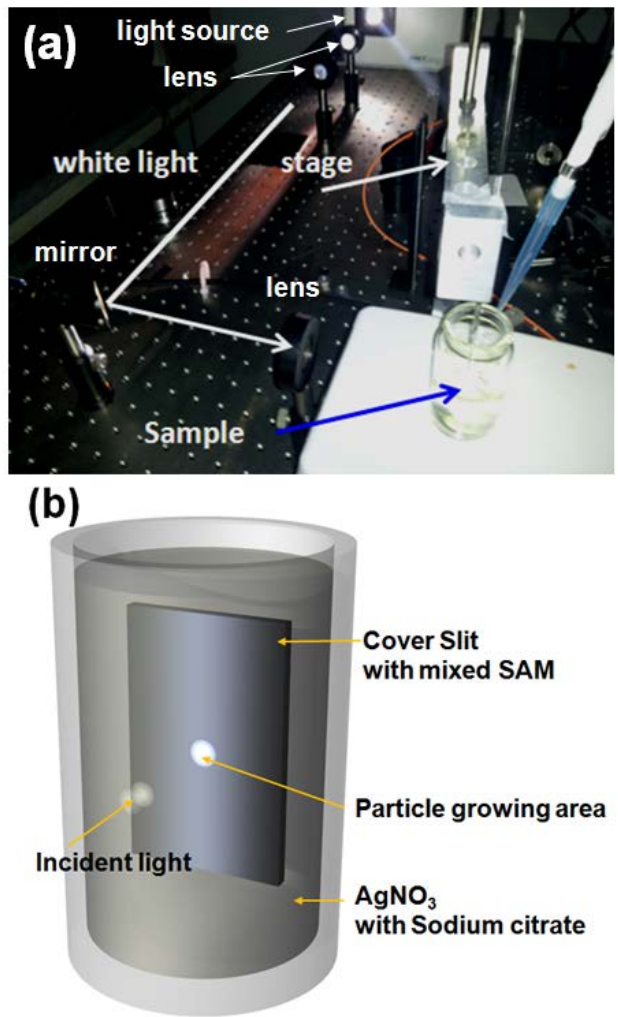

Figure III-2. Photo-reduction system. (a) Real image of the system. (b) Schematic diagram of photo-reduction process.

I.2.2. Dark field microscopy

A homemade dark field (DF) microscopy was used to monitor the dark field image and the scattering spectrum from the samples.

The system consists of two parts. One is the DF image and spectrum detection part and the other one is the SERS spectra detection part. Scheme III-1 shows the general schematic diagram of the system.

For DF image and scattering spectrum, microscopy (Nikon Eclipse, TE2000-s), DF condenser (Nikon, T-CHA, oil 1.43-1.20), CCD camera (Nikon, DS-Fi1), and photomultiplier tube (Acton Research, PD-471) were aligned and calibrated. The CCD was used to monitor DF images and the photomultiplier tube was used to observe extinction spectra. A halogen lamp (Nikon, LHS-H100P-1) was used as a photo-illumination source and a ×100 oil type objective lens (Nikon, Plan Flour, WD = 0.16, 0.5-1.3 NA oil iris) was used to collimate the scattered light from the sample. Figure III-2 shows real image of the DF microscopy system. Figure III-3 (a) is the DF image and spectra detection part and (b) is the SERS spectra detection part.

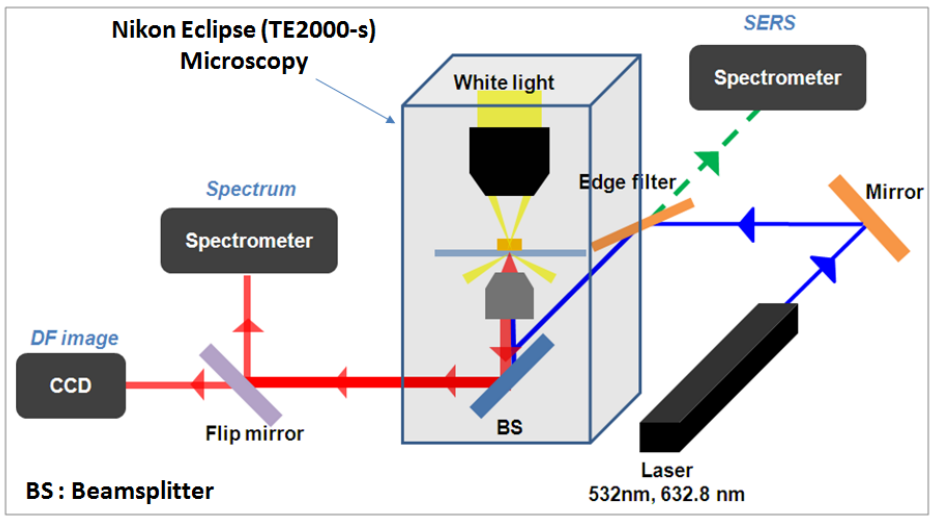

Scheme III-1. General schematic diagram of the dark field (DF) microscopy system. The CCD was used to monitor DF images and the PMT was used to observe extinction spectra. A halogen lamp was used as a photo-illumination source and a ×100 oil type objective lens was used to collimate the scattered light from the sample.

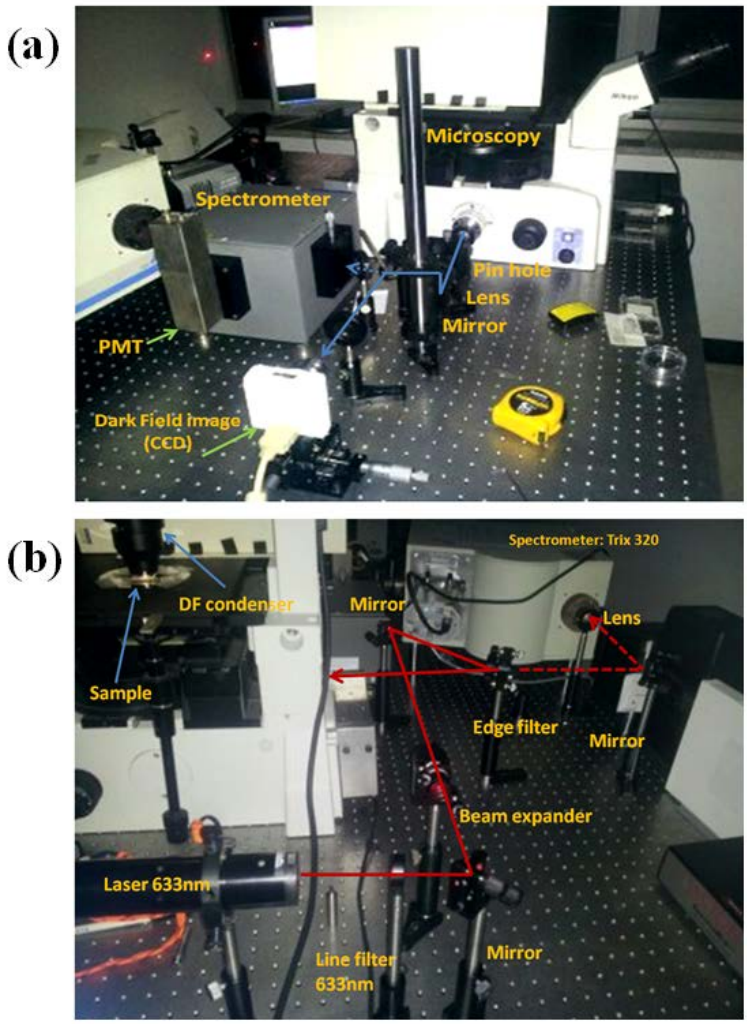

Figure III-3. Real image of the DF microscopy system. (a) is the DF image and extinction spectrum detection part and (b) is the SERS spectra detection part.

I.3. Preparation of the mixed SAM layer on the glass substrate

In order to form mixed SAM layer on a glass substrate, the substrate was cleaned by acetone and then distilled water with sonication for 20min. The glass substrate was then activated with hydroxyl functional groups by dipping it into a piranha solution for 20 min which was composed of H_2SO_4 and H_2O_2 in a 4:1volume ratio. The glass substrates were then rinsed with absolute ethanol and further rinsed with distilled water and dried under nitrogen.

APMES serves as the growing site of silver nanoparticles as the amine group has affinity to silver metals while TMS has less affinity. Hence, by mixing two silane coupling reagents, the distribution of amine groups on the glass substrate was controlled. In order to investigate the nanoparticle growing ability on the ratio of mixed SAM formed substrates, the activated silica substrates were immersed into the mixture of APMES and TMS during 90min. The glass substrates were then washed with isopropyl alcohol and distilled water 3 times, respectively and dried under nitrogen. Substrates with five different mixed ratios of APMES and TMS (1:0, 1:10, $1:10^2$, $1:10^3$ and $1:10^4$) were used.

I.4. Silver nanoparticle growing by photo-reduction

Figure III-4 shows a schematic illustration of the photo-induced growing process on a glass substrate. Prior to growing Ag NPs, the substrate surface was functionalized with a mixture of APMES (amine functionalized silane) and TMS (non-amine functionalized silane) to control the surface proportion of amine-coupling group since silver has stronger affinity to amine group than TMS group. Then, the substrate was dipped in the reaction solution where 20 ml of 1 mM silver nitrate solution and 0.5 ml of 1% (w/v) sodium citrate solution were mixed and a focused beam of white light (*ca.* 4mm diameter) was illuminated on the substrate (Figure III-3(b)). At the initial stage silver nanoparticle seeds that are produced within the light illuminated region would bind to the amine-groups on the surface as shown in Figure III-4(c), and then subsequent photo-reduction would occur preferentially near the seeds since the localized and enhanced optical field are created near the silver nano-seeds due to surface plasmon resonance of the silver nano-particles. In order to find optimum condition of Ag NP growing in respect of mono-dispersity, mean diameter and particle density, the mixed SAM ratio of APMES and TMS, photo-illumination time, and the concentration of Ag growing solution were varied as control factors.

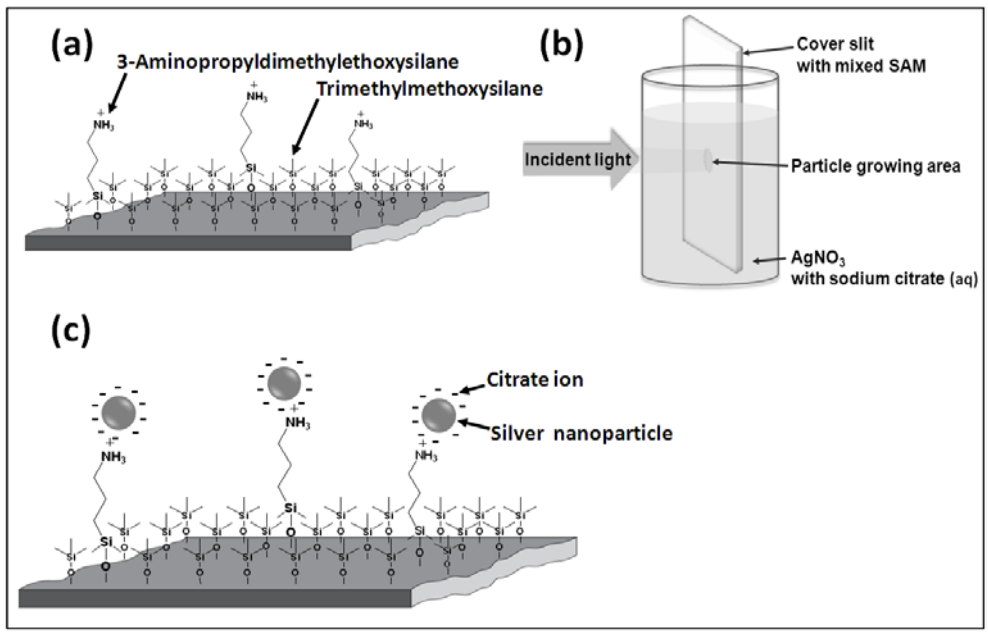

Figure III-4. Schematic illustration of the Ag NP growing process on a glass substrate with photo-reduction. (a) Molecular configuration of the substrate surface after silanization with a mixture of APMES and TMS. (b) Experimental setup to obtain photo-induced growing of Ag NPs on the substrate. A white-light beam from a Xenon lamp was focused on the substrate in the reaction solution. The diameter of the focused area was *ca*. 4 mm. (c) Illustration of the substrate surface at the initial stage of growing Ag NPs on the silica substrate by photo-illumination.

I.5. Scanning electron microscope (SEM) measurements

After photo-reduced growing the morphologies of the samples were measured with a field-emission scanning electron microscope (FE-SEM, Carl Zeiss, SUPRA 55VP). Obtaining the clear SEM images, samples should be electrically grounded. Therefore, before the SEM measurements, all samples were coated with platinum using “Hummer VI” sputter deposition system. Around 35 angstrom thick platinum will coated during 1.5 min coating based on the specification of the instrument.

II. Results and discussion

II.1. Light intensity profile

A focused beam of white-light illumination has an intensity profile of a Gaussian distribution. Hence, while keeping all other experimental conditions constant, illuminated light power at the surface is not the same over the surface and hence, this effect on Ag NPs growing was characterized.

For this characterization, a glass substrate was activated with hydroxyl functional groups by dipping it in the piranha solution for 20min and subsequently in 1mM APMES coupling solution for 90 minutes. Light illumination time was 30min. A mixture of 20 ml, 1 mM silver nitrate and 0.5 ml, 1% (w/v) sodium citrate was used as a nanoparticle growing solution.

Figure III-5 shows SEM images exhibiting growing patterns of Ag NPs at various sites with different light power density. The diameter of the light illuminated region was estimated to be approximately 4mm. For the FE-SEM measurements five different spots were chosen over the entire light illuminated region representing the site of highest illumination (Spot 3) to little illumination (Spots 1 & 5). The top-left image in Figure III-5 is a low

magnified one showing the entire region of light illumination, and the others are high magnified ones at the designated spots, respectively. The silver density is the highest at the center (Spot 3) and becomes lower to the distant site from the center (Spot 1 & 5). Therefore, the central site was chosen to investigate growing characteristics of Ag NPs on glass substrates in the following experiments.

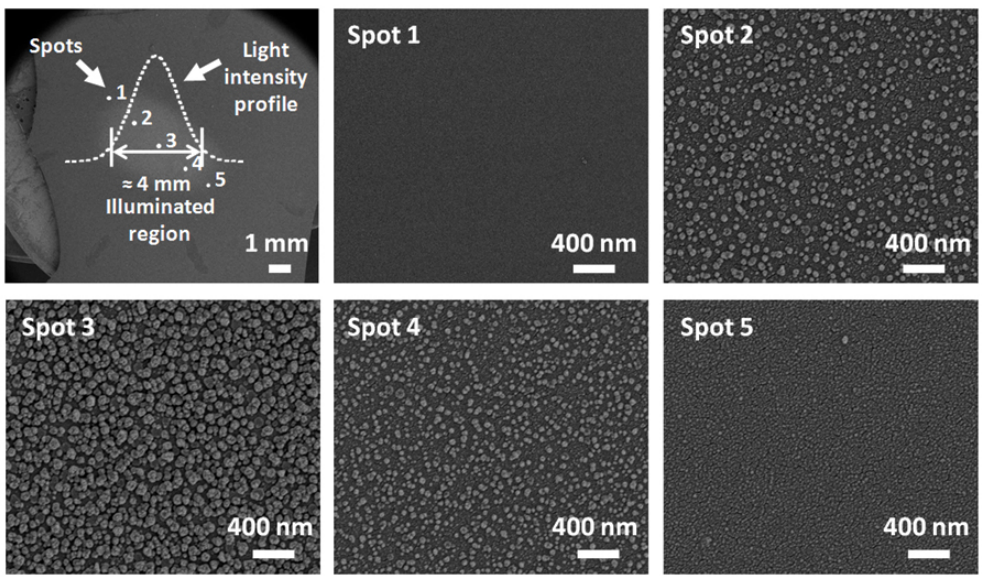

Figure III-5. FE-SEM images of grown Ag NPs on the APMES treated glass with 30 min light illumination. The top-left image is a low magnified image showing the entire region of light illumination, and the others are high magnified images at the designated spots, respectively. Spot 3 is the central spot with the highest light illumination and the spots 1 and 5 are the ones far from the center.

II.2. The mixing ratio of APMES and TMS coupling reagents

As an effort to make mono-disperse Ag NPs on the substrate, a mixed SAM of APMES and TMS coupling reagents is chosen since APMES can serve as a silver-growing site through amine-functional group while TMS group is not adhesive to silver. In order to investigate the growing characteristics of the silver nanoparticles on the mixed SAM layer assembled substrates, five different mixing ratios of APMES and TMS coupling reagents were chosen from 1:0, 1:10, $1:10^2$, $1:10^3$ to $1:10^4$. The glass substrate was treated with the silane-coupling solution for 90 min. For all experiments, photo-illumination time was 30 min and a growing solution that was mixed with 20 ml of 1 mM silver nitrate and 0.5 ml of 1% (w/v) sodium citrate was used.

Figure III-6 shows FE-SEM images of the photo-induced grown Ag NPs on glass substrates treated with different mixed silane-coupling reagents ratios. The each FE-SEM images were measured center of the whole light illuminated region which was the highest grown Ag NPs and a total area of the each images were 9 μm^2.

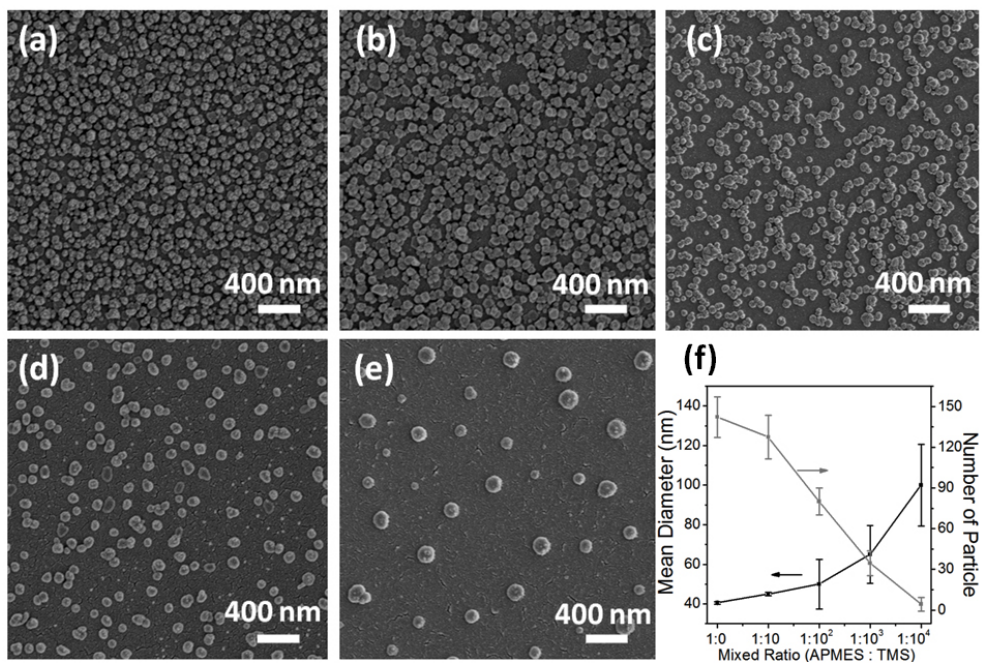

Figure III-6. FE-SEM images of the photo-induced grown Ag NPs on glass substrates prepared with various mixed silane-coupling reagents ratios. From (a) to (e) the mixing ratios of APMES and TMS coupling reagents were 1:0, 1:10, $1:10^2$, $1:10^3$ and $1:10^4$, respectively. (f) The plots of Ag NP's mean diameter and number of particles within 9 μm^2on the mixing ratio of APMES and TMS.

Figure III-6(a) shows glass substrate was treated with only 1 mM APMES silane-coupling solution for 90 min. The all concentration of the mixed coupling solutions and times are the same as the one in Figure III-6(a) but the mixed ratios of APMES and TMS solutions are 1:10, $1:10^2$, $1:10^3$ and $1:10^4$ for Figure III-5(b), (c), (d), and (e), respectively.

The density of amine groups on the glass substrate depends on the mixing ratio of APMES and TMS. The FE-SEM images indicate that the population of Ag NPs on the substrates decreased as the ratio of APMES coupling reagents decreased. In the case of the higher ratio of APMES the surface density of Ag NPs was higher while contact and merging between particles also increased during the growing process (Figure III-6(a)). However, in the case of the lower ratio of APMES amine groups on the substrate were far from one another and hence particles were grown well separated while their mean diameter was also increased (Figure III-6(e)). This result implies that the density of the amine functional groups on the glass substrate can control of the density and size of Ag NPs on the substrate.

The FE-SEM images of the entire illuminated region shows in Figure III-7. Overall experiments light illumination times were 30 min and mixture of 20 ml, 1 mM silver nitrate and 0.5 ml, 1% (w/v) sodium citrate was used.

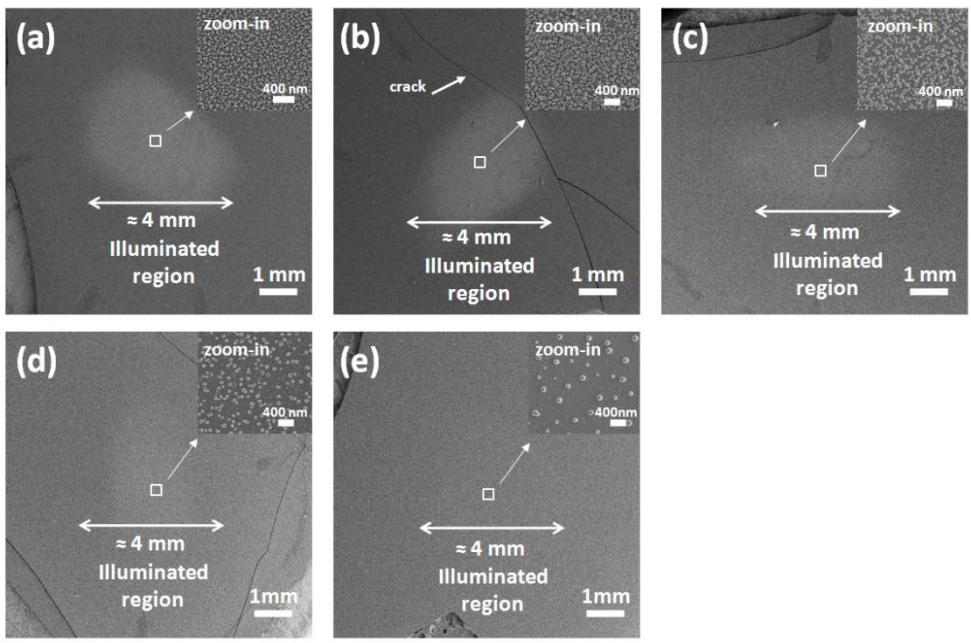

Figure III-7. Low magnified SEM images of the photo-reduced grown Ag NPs on glass substrates treated with different mixed silane-coupling reagents ratios. (a) The glass substrate was treated only with 1 mM APMES coupling solution for 90 min. The all concentration of the mixed coupling solutions and times are the same as the one in (a) but the mixed ratios of APMES and TMS solutions are 1:10, $1:10^2$, $1:10^3$ and $1:10^4$ for (b), (c), (d), and (e), respectively.

After photo-reduced growing experiment of the Ag NP, Energy-dispersive X-ray (EDX) (Carl Zeiss SUPRA 55VP spectrometer) analysis were also performed, in order to confirm whether the grown particles are Ag NPs or not. Figure III-8(a) shows SEM image of the EDX analyzed area and (b) is the EDX spectrum. There are platinum and aluminum picks on the EDX spectra, because of the sample preparation method such as platinum coating, aluminum foil keeping of samples. According to the result of the EDX spectra, we concluded that the Ag NPs were well grown on the substrate.

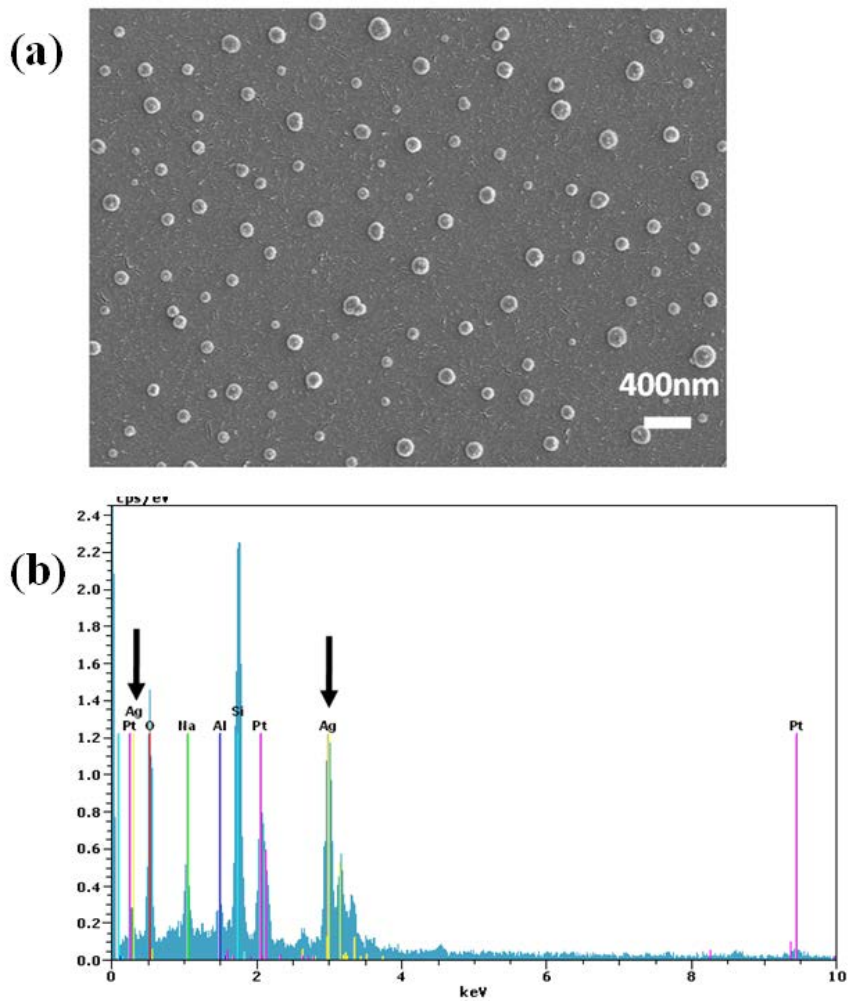

Figure III-8. EDX analysis of the photo-reduced grown silver nanoparticles on glass substrates treated with silane-coupling reagents of APMES:TMS ratio of $1:10^4$. (a) Shows SEM image of the EDX analyzed area and (b) is the EDX spectrum.

As one of optical characterization tools DF microscopy was employed to detect light scattering of Ag NPs due to localized surface Plasmon resonance. Figure III-9 shows the DF images of the Ag NPs on the glass substrate treated with the mixed silane-coupling solution (APMES and TMS mixed ratios of 1:0, 1:10, $1:10^2$, $1:10^3$, and $1:10^4$, respectively). When the ratio of APMES is high, small particles were highly populated and mutually merged, and bright particles were not individually distinguished. As the APMES ratio decreases, bright particles became well separated and their colors changed from multi-color feature to rather monotonous color representing mono-disperse nature of Ag NPs.

In order to get further insights on their optical features extinction spectrum was obtained. The measured extinction spectrums were shown in Figure III-10(a) and Figure III-10(b) shows extinction spectrums maximum points and spectrum bandwidth changes with the grown Ag NPs on glass substrates treated with various mixed silane-coupling reagents APMES and TMS ratios of 1:10, $1:10^2$, $1:10^3$ and $1:10^4$.

The extinction maximum appeared at 563nm in the case of the highest APMES ratio and shifted gradually to blue with a decrease of the APMES ratio while its bandwidth also decreased. This feature is consistent with the

optical features shown in the DF images and the morphological features shown in the FE-SEM images.

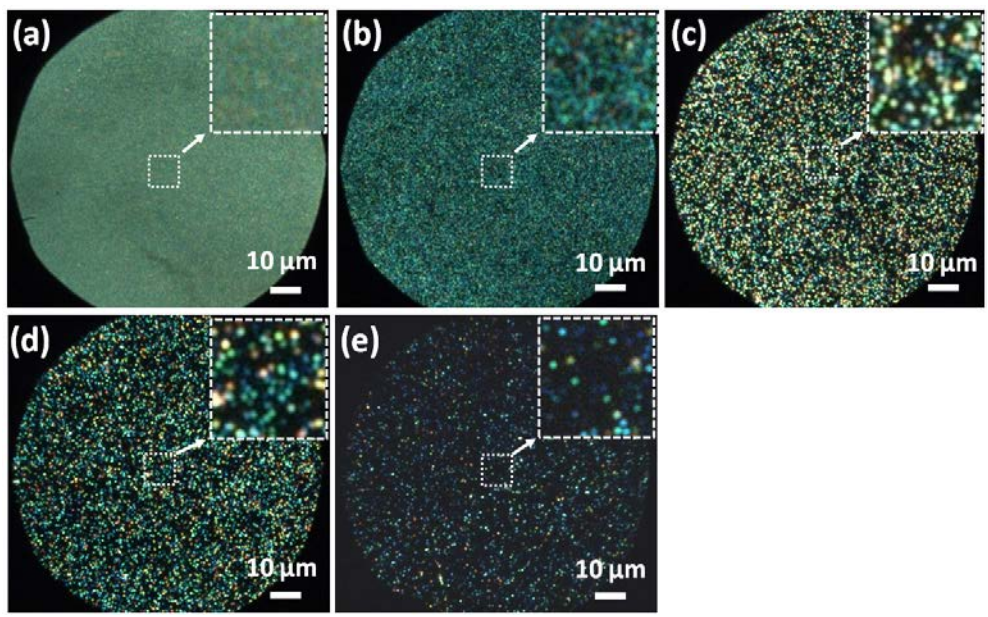

Figure III-9. DF images of the photo-reduced Ag NPs on glass substrates treated with silane-coupling reagents of various mixing ratios. From (a) to (e) the mixing ratios of APMES and TMS coupling reagents were 1:0, 1:10, $1:10^2$, $1:10^3$ and $1:10^4$, respectively. Inset of the each figure show zoom in image of the 9 μm^2 area which is the center spot with the highest light illumination.

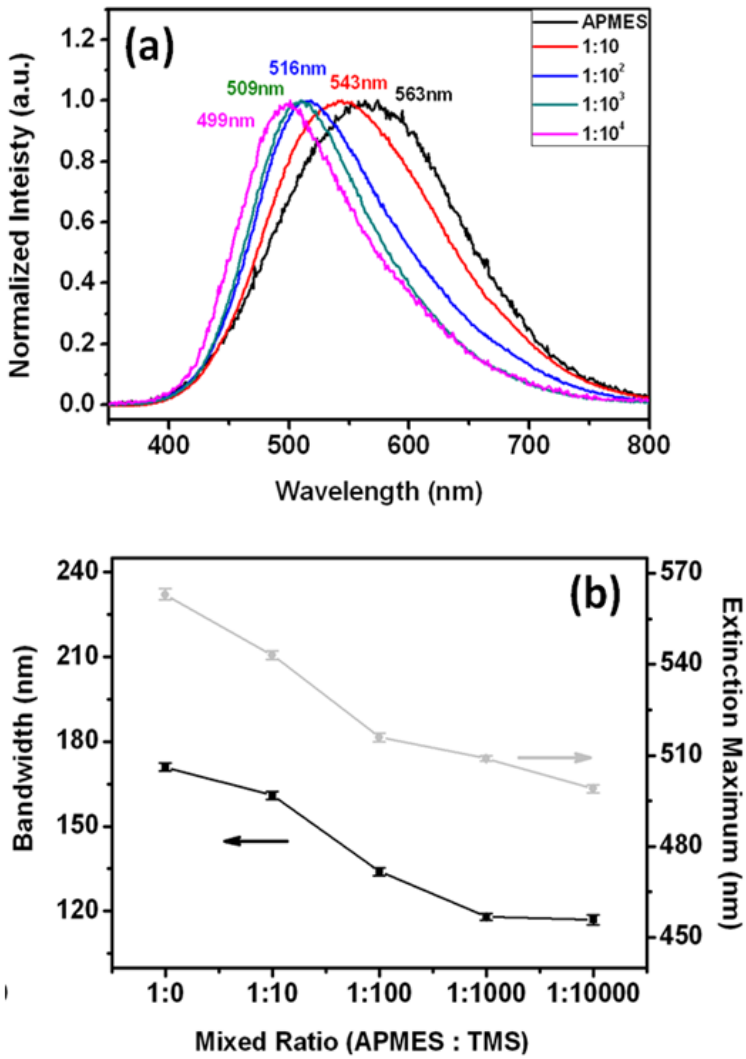

Figure III-10. Extinction spectrum changes of the grown Ag NPs on the glass substrates covered with various mixed SAM. (a) The measured extinction spectrum. (b) Extinction spectrum maximum points and spectrum bandwidth change.

II.3. Effect of photo-reduction time on silver nanoparticle growth

As one of factors controlling mono-disperse growing, Ag NPs were grown with different photo-reduction time (15, 30, 45, 60, 75, 90, and 120 min). For this experiment the $1:10^4$ ratio of APMES and TMS was chosen for growing NPs from the results shown in Figure III-6(e).

The FE-SEM images of the entire photo-reduced region shows in Figure III-11. Overall experiments mixture of 20ml, 1mM silver nitrate and 0.5 ml, 1% (w/v) sodium citrate were used. But the photo-reduction times were 15, 30, 45, 60, 75, 90 and 120 min for (a), (b), (c), (d), (e), (f) and (g) respectively.

Figure III-12 shows high magnified FE-SEM images of the Ag NPs with different photo-reduction times. As the photo-reduction time increased, the particle size and the particle density increased asymptotically, indicating that the seeding sites on the substrate surface were saturated with photo-reduction time. When the photo-reduction time is short, Ag NPs grew almost as monomers as shown in Figure III-12(a) and (b). However, with the longer photo-reduction the degree of monomer became reduced as shown in Figure III-12(c), (d), (e), (f) and (g). Until 30 min high mono-

dispersity could be obtained. Therefore, for the following experiments the samples were fabricated with the $1:10^4$ ratios of APMES and TMS and 30 min photo-illumination.

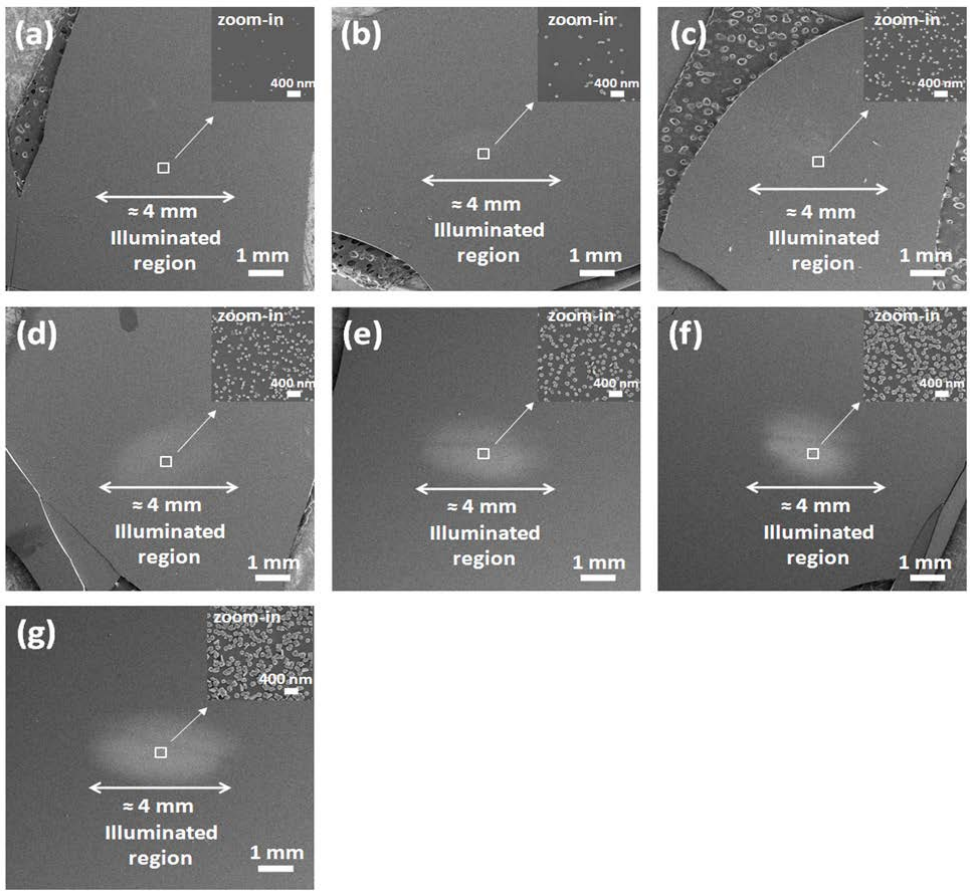

Figure III-11. The FE-SEM images of the entire illuminated region of the photo-reduced grown Ag NPs on glass substrates treated with mixed coupling reagents (APMES:TMS) ratio of $1{:}10^4$ with different light illumination times. Overall experiments mixture of 20ml, 1mM silver nitrate and 0.5 ml, 1% (w/v) sodium citrate were used. Light illumination times were 15, 30, 45, 60, 75, 90 and 120 min for (a), (b), (c), (d), (e), (f) and (g), respectively.

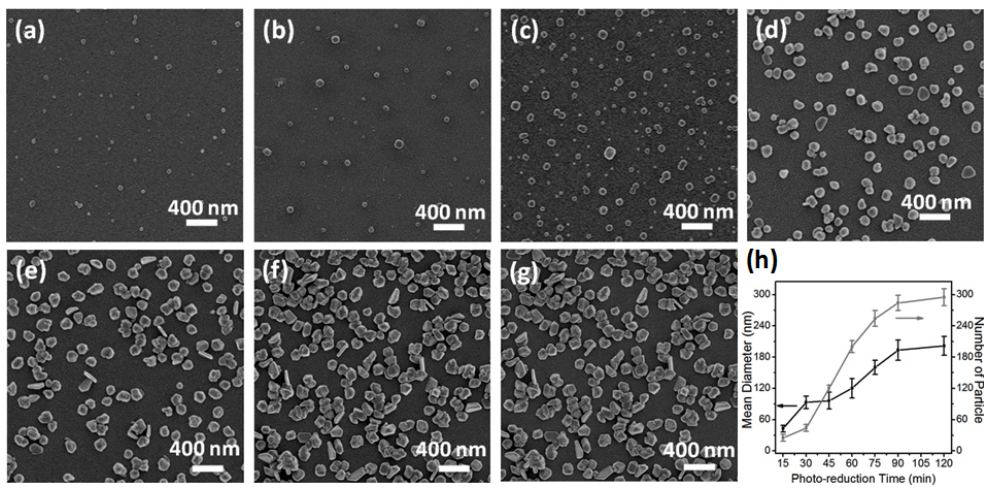

Figure III-12. FE-SEM images of the photo-reduced Ag NPs on glass substrates treated with silane-coupling reagents APMES and TMS (mixed ratio of $1:10^4$) with various photo-reduction time. Photo-reduction time was 15, 30, 45, 60, 75, 90 and 120 min from (a) to (g), respectively. (h) The plots of Ag NP's mean diameter and number of particles within 9 μm^2 on photo-reduction time. For the overall experiment the mixture of 20 ml, 1 mM silver nitrate and 0.5 ml, 1% (w/v) sodium citrate were used.

II.4. Effect of the silver growing solution on nanoparticle growth

Growing of the Ag NPs on glass substrates were controlled by the concentration of silver nitrate solution. Figure III-13 shows the FE-SEM images of the entire photo-reduction region. For each experiment a mixture of 20ml silver nitrate (0.001, 0.01, 0.1, 1 and 10 mM) and 0.5 ml, 1% (w/v) sodium citrate solution was used for photo-reduction of Ag NPs using the substrate that was treated with a mixed coupling agent of APMES and TMS (ratio of $1:10^4$). For all experiments, photo-reduction time was 30 min.

The high magnified FE-SEM images are also shown in Figure III-14. FE-SEM images exhibit the growth patterns of Ag NPs using different concentrations of silver nitrate solution from 0.001, 0.01, 0.1, 1 to 10mM. The growing rate of Ag NPs increased dramatically when the concentration of the growing solution increased from 0.001 mM to 10 mM.

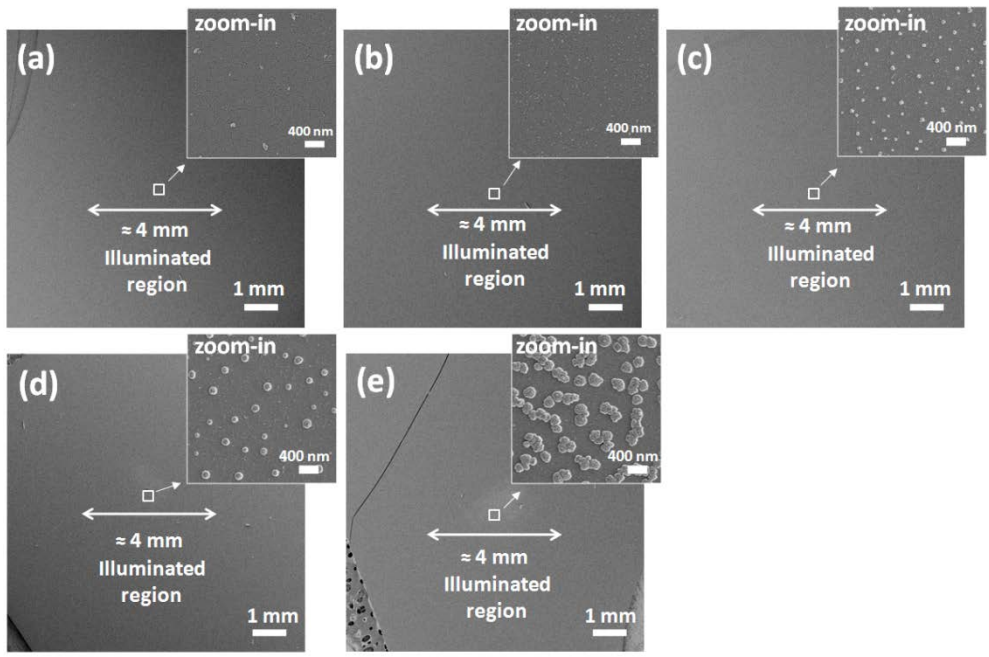

Figure III-13. The FE-SEM images of the entire illuminated regionof the photo-reduced grown Ag NPs on glass substrates treated with mixed coupling reagents (APMES:TMS) ratio of $1:10^4$ with different silver nitrate concentrations. Overall experiments light illumination time was 30min and mixture of 0.5 ml, 1% (w/v) sodium citrate and 20 ml silver nitrate was used. The silver nitrate concentrations were 0.001, 0.01, 0.1, 1 and 10 mM for (a), (b), (c), (d), and (e), respectively.

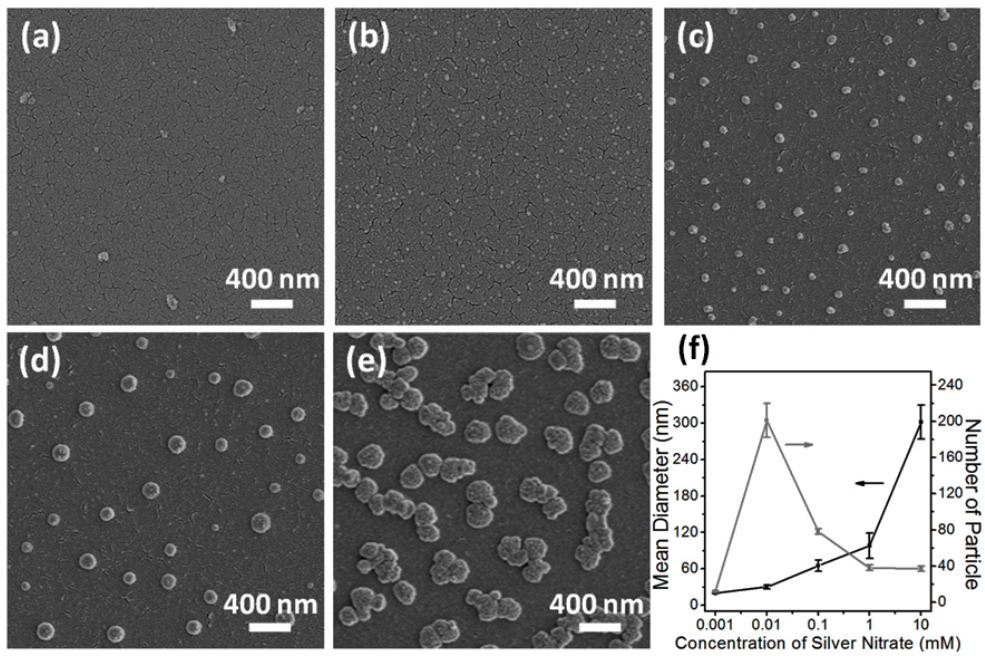

Figure III-14. FE-SEM images of Ag NPs on silica substrates with different silver nitrate concentrations. The substrate was treated with a mixed coupling agent of APMES and TMS (ratio of $1:10^4$) and photo-reduction time was 30 min for all experiments. Mixture of 0.5 ml, 1% (w/v) sodium citrate and 20 ml silver nitrate was used. The concentration of silver nitrate solutions were 0.001, 0.01, 0.1, 1, and 10 mM for (a), (b), (c), (d), and (e), respectively. (f) The plots of Ag NP's mean diameter and the number of particles within 9 μm^2 on the concentration of silver nitrate solution.

The growth of Ag NPs was analyzed in respect of three different factors (the mixed ratio of silane-coupling reagents, the photo-reduction time, and the concentration of growth solution shown as in Figure III-6, 12, and 14, respectively). In order to understand fabrication condition of Ag NPs with high mono-dispersity and high coverage, mean diameter, surface coverage, and degree of monomer growth were depicted in terms of the three factors. Surface coverage is defined as the ratio of the covered area of Ag NPs to the total surface area, and degree of monomer is defined as total area of monomers divided by the covered area of Ag NPs.

As the mixed ratio of APMES to TMS decreases, the mean diameter of Ag NPs increased from 40 nm to 100 nm and the surface coverage decreased from 0.78 to 0.062 while the degree of monomer increased drastically due to the far distant distribution of amine groups on the surface (Figures 6 (a), (b), &(c)). The degree of the monomers were 0.004 ± 0.008 , 0.024 ± 0.007, 0.089 ± 0.007, 0.436 ± 0.014, and 0.963 ± 0.014 for the APMES and TMS mixed ratios of 1:0, 1:10, $1:10^2$, $1:10^3$, and $1:10^4$, respectively. According to the results (shown in Figure III-12(a), (b), and (c)), using the $1:10^4$ mixed ratio of silane-coupling reagents, we obtained highly mono-disperse Ag NPs of 100 ± 20 nm size grown on the silica

substrate which has high degree of monomer of 0.963, and 6.2% surface coverage. This substrate was chosen for the following study.

Figure III-12(d), (e), & (f) show the effect of photo-reduction time on nanoparticle growth using the $1:10^4$ mixed ratio of APMES and TMS and the 1 mM silver nitrate solution. Photo-reduction time was varied from 15, 30, 45, 60, 75, 90, and 120 min. With the photo-reduction time, the mean diameter increased from 42 nm to 201 nm and the surface coverage increased slowly from 0.006 to 0.768 while the degree of monomer decreased steeply from 45min due to overlaps between enlarged particles. In order to maintain high mono-dispersity, 30min illumination or less was suitable.

With a concentration increase of silver nitrate solution the mean diameter and the surface coverage increased monotonically keeping mono-dispersity until 1mM concentration while at 10mM concentration a drastic increase of the mean diameter and the surface coverage occurred with a subsequent decrease of mono-dispersity (Figure III-14(g), (h), & (i)). Based on these results, the concentration of 1mM or less is suitable to get high mono-dispersity.

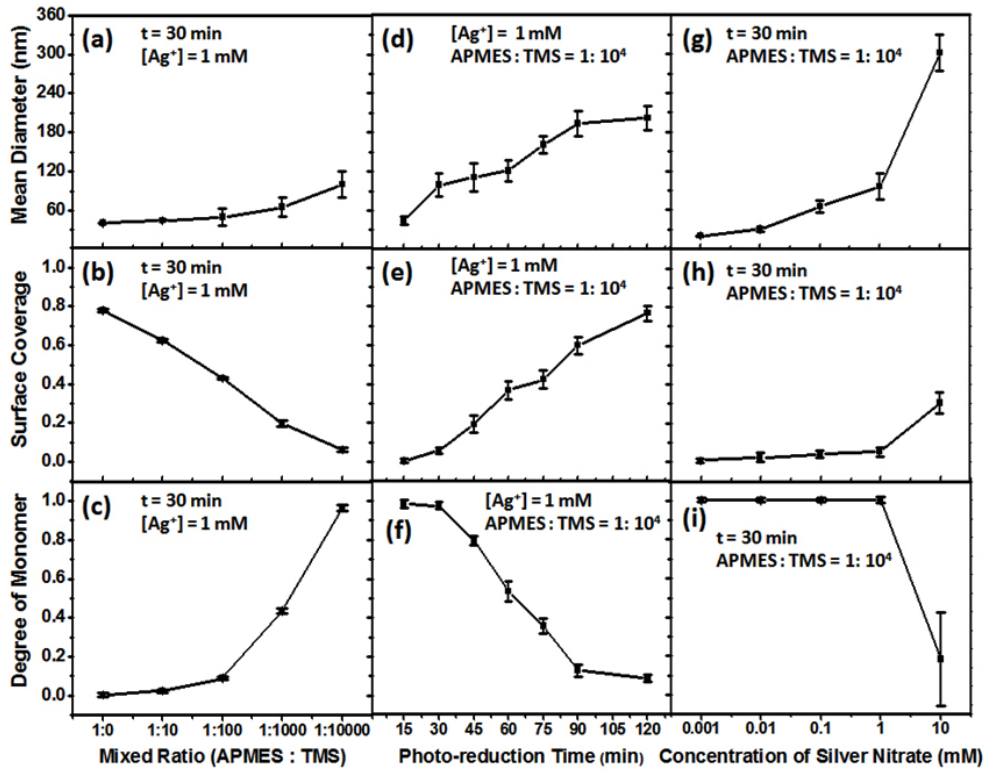

Figure III-15. Growing characteristics of Ag NPs. The dependence on the mixed ratio of APMES and TMS is shown in (a), (b), and (c). The photo-reduction time was 30 min and the silver nitrate concentration was 1mM. The dependence on the photo-reduction time is shown in (d), (e), and (f). The silver nitrate concentration was 1mM and the mixed ratio of APMES and TMS was $1:10^4$. The dependence on the silver nitrate concentration is shown in (g), (h), and (i).

II.5. Interpretation of the silver nanoparticle growing by photo-induced reduction

We have conducted various experiments by changing the mixed ratio of silane-coupling reagents, the photo-illumination time, and the concentration of the silver nitrate solution. From the results, we obtained detailed information related to the growing of Ag NPs on glass substrates covered with mixed silane-coupling reagents of APMES and TMS. Getting the clear vision of the photo-induced growing process there are two mechanisms can be considered.

Mechanism 1: Seeds form in solution → They are attached on substrate surface → Growing on surface prevails while seedscan be created in solution.

Mechanism 2: Seeds form and grow in solution →They are attached on substrate surface

According to Mechanism 1, at the initial stage reduction of Ag+ ions to Ag0 silver occurs in the solution within the light illumination and instantly the neutral silvers will form small seeds with adsorption of anions such as citrate to stabilize its surface energy. Then, the small Ag seeds with negative

surface charge are attracted and bound to positively charged amine groups on a substrate. Further growing of Ag nanoparticles from the seed particles on the substrate prevails due to the localized and intensified optical fields close to the seeds while seeds can be still created in solution.

According to Mechanism 2, silver seeds form and grow in solution and then some of them attached to positively charged amine groups on a substrate.

In order to find clues on the probable mechanism we performed a control experiment of nanoparticle fabrication under the following conditions. The mixture of 20 ml, 0.001 mM $AgNO_3$ and 0.5 ml, 1 % (w/v) sodium citrate was used as a silver nanoparticle growth solution. This solution was illuminated for 30 min without the APMES treated substrate. Then the APMES-treated substrate with mixed ratio of APMES and TMS being 1:104 was dipped in this solution for additional 30 min without further photo-illumination. SEM image of this substrate is shown in Figure III-16. This data shows that silver nanoparticles grow in solution by photo-illumination even without substrate and the size is ca. 6 nm in average. This size is much smaller than the smallest particles of ~20 nm (Fig. III-15 (g)) and also larger than seed particles of a few nanometer [111].

This reflects that in solution by photo-illumination silver nanoparticle can still grow from its seeding size and can have chance to attach on the substrate further, but however the size is much smaller than the particles that grew directly from the attached particles on the substrate. In Figure III-14 (c) & (d), small variation of particle size on substrate surface can be observed. This can be understood that the early formed seeds, once attached on surface, grow larger and the lately formed seeds grow smaller on surface.

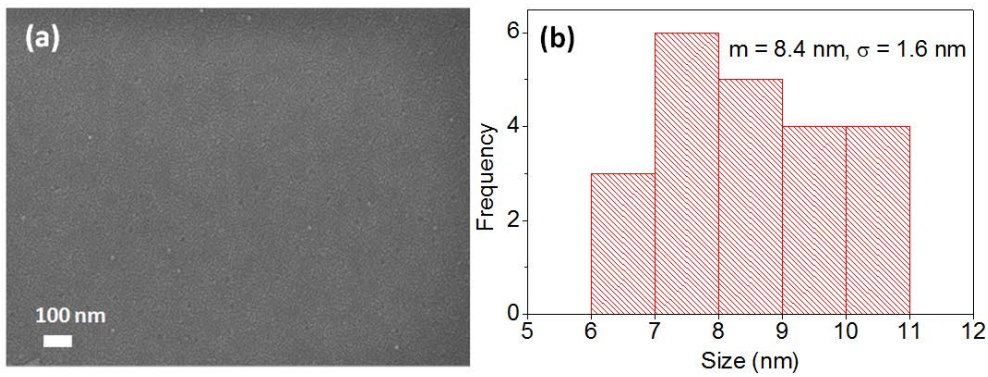

Figure III-16. Silver nanoparticles were grown in a mixture of 20 ml, 0.001 mM $AgNO_3$ and 0.5 ml, 1 % (w/v) sodium citrate by photo-illumination for 30 min without an APMES treated substrate. Then, the APMES-treated substrate with mixed ratio of APMES and TMS being $1:10^4$ was dipped in this solution for additional 30 min without further photo-illumination in order to obtain SEM images of silver nanoparticles attached on this substrate after grown in solution. (a) The SEM image of silver nanoparticles attached on the substrate. (b) The histogram of the measured particle size, which gives size = 8.4 ± 1.6 nm in average. If Pt coating of ~2 nm during SEM measurement, the average size can be estimated to be *ca.* 6 nm. Due to the resolution limit of SEM measurement, the smaller particles may not be included in this estimation even though they exist.

As an effort to find evidence of in-solution growing of silver nanoparticles during on-surface growing with photo-illumination, we performed following experiments and analysis using the same growth solution in Figure III-16 (the mixture of 20 ml, 0.001 mM $AgNO_3$ and 0.5 ml, 1 % (w/v) sodium citrate). Photo-reduced growing was performed for 30 min using APMES-treated substrate (in this case, only APMES was treated to prepare highly grown substrate for comparison). In comparing the UV-Visible extinction spectra of the growth solutions before and after photo-reduced growing (Figure III-17 (a)), no significant difference was observed. However, in the SEM image of the APMES-treated substrate highly grown silver nanoparticles were clearly observed in Figure III-17 (b), and in the TEM image from the growth solution after photo-reduced growing the smaller silver nanoparticles of a broad size range can be monitored (Figure III-17 (c)) even though we cannot see any spectral difference in Figure III-17 (a). This result indicates that silver particles grow predominantly on the substrate surface while relatively small amount of growing in solution still occurs but spectroscopically insignificantly.

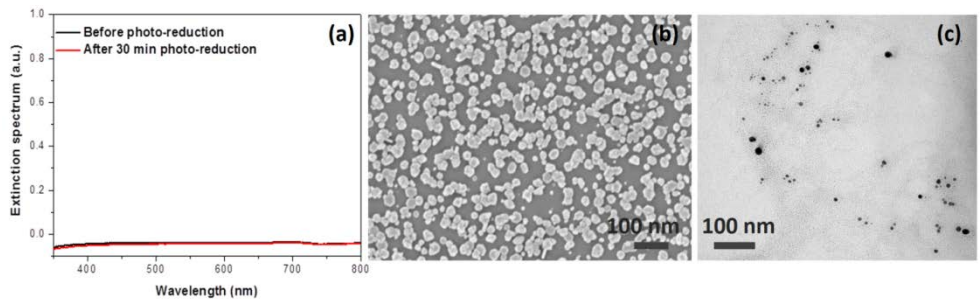

Figure III-17. Comparison experiment of photo-induced growing in substrate surface and growth solution, we performed following experiments and analysis using the same growth solution in Figure S6 (the mixture of 20 ml, 0.001 mM $AgNO_3$ and 0.5 ml, 1 % (w/v) sodium citrate). Photo-reduced growing was performed for 30 min using APMES-treated substrate (in this case, only APMES was treated to prepare highly grown substrate for comparison). (a) UV-Visible extinction spectra of the growth solutions before and after photo-reduced growing. (b) SEM image of the APMES-treated substrate showing highly grown silver nanoparticles on the substrate. (c) TEM image from the growth solution after photo-reduced growing showing the smaller silver nanoparticles of a broad size range.

For exact interpretation of the growing process the following experiments also performed. The experimental conditions were the same as in the Figure III-17 except substrate treatments. Two substrates were prepared: One is the substrate of which surface was activated by the Piranha solution for 20 min, and the other is the substrate of which surface was 1 mM TMS treated. SEM images of the both sample were shown in Figure III-18. Both samples have almost no particles on the surface in a wide view. In some local area, small clusters of silver nanoparticles are monitored in the non-silanised substrate as in Figure III-18 (a) while no particles are monitored in the TMS-treated substrate. Figure III-19 shows the mechanism of the photo-reduced growing process.

In summary, even though silver nanoparticles can form and grow in solution with photo-illumination, their amount is not as much as the amount grown on surface and their size and shape cannot explain the well-controlled pattern of silver nanoparticles on surface. Silver particles can grow in solution but once they are attached on the amine-functionalized site of surface substantial growing is induced due to intensified local fields close to the silver nanoparticles on surface.

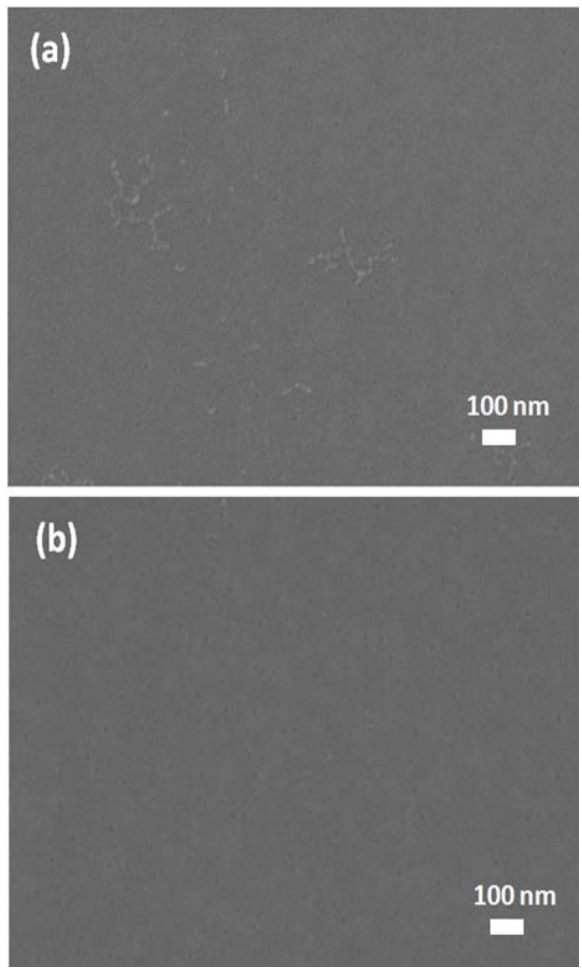

Figure III-18. SEM images of the substrates after photo-reduced growing for 30 min. Experimental condition is the same as in Figure III-17 but substrate treatment is different. (a) The substrate is treated with only Piranha solution. (b) The substrate is treated with TMS-silanised substrate.

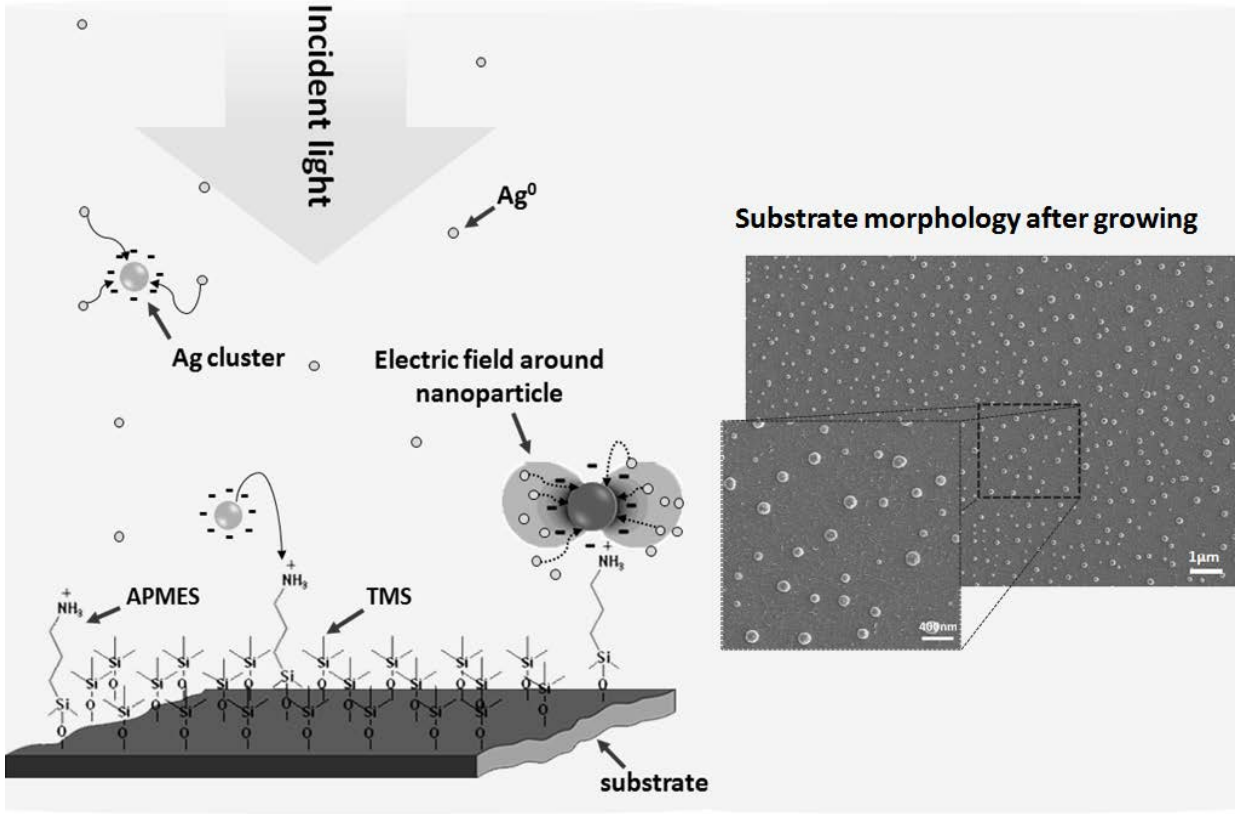

Figure III-19. Mechanism of the photo-reduced growing process.

II.6. The Result of Photo-induced Growing on Fiber Optics

According to the Photo-induced nanoparticles growing on glass substrate, we were tried to identify most suitable growing parameters such as photo-reduction time, concentrations of growth solution and mixed ratio of APMES and TMS for substrate preparation. The best parameters for uniform growing was founded as: 30 min photo-reduction, mixture of 20 ml, 0.001 mM $AgNO_3$ and 0.5 ml, 1 % (w/v) sodium citrate as a silver nanoparticle growth solution and the APMES-treated substrate with mixed ratio of APMES and TMS being $1:10^4$. For the photo-induced growing on FO these parameters were used. Figure III-20 shows the main experimental diagram of photo-induced growing on FO. Around 15 cm long FO was cut and its protecting polymer cover was removed around 4 cm long from both ends. Then, both ends were cleaved to expose a smooth silica surface using fiber optic cleaver (FITEL S325, Furukawa Electric) and the surface smoothness was checked using a fusion splicer. On the one end of the FO mixed SAM layer was prepared (APMES:TMS = $1:10^4$) same as explained in Chapter III, Section I.3. From the opposite end, light from the Xenon

lamp was focused through using ×10 objective lens (Olympus, 0.25 NA, WD=10.6 mm).

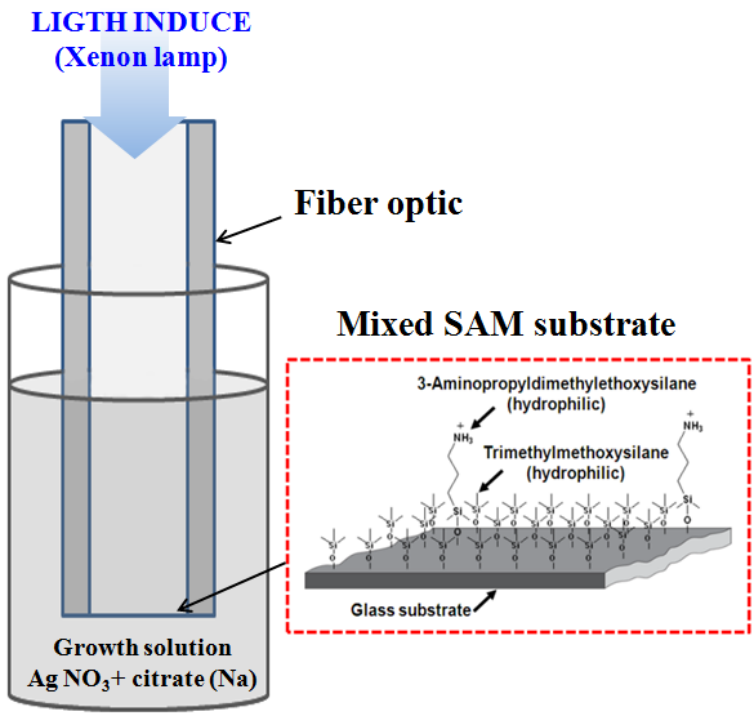

Figure III-20. Experimental diagram of photo-induced growing on FO. Around 15 cm long FO was used. Both ends of the FO were cleaved to expose a smooth silica surface using fiber optic cleaver (FITEL S325, Furukawa Electric). On the one end of the FO mixed SAM layer was prepared (APMES:TMS = $1:10^4$) same as explained in Chapter III, Section I.3. From the opposite end, light from the Xenon lamp was focused through using ×10 objective lens (Olympus, 0.25 NA, WD=10.6 mm).

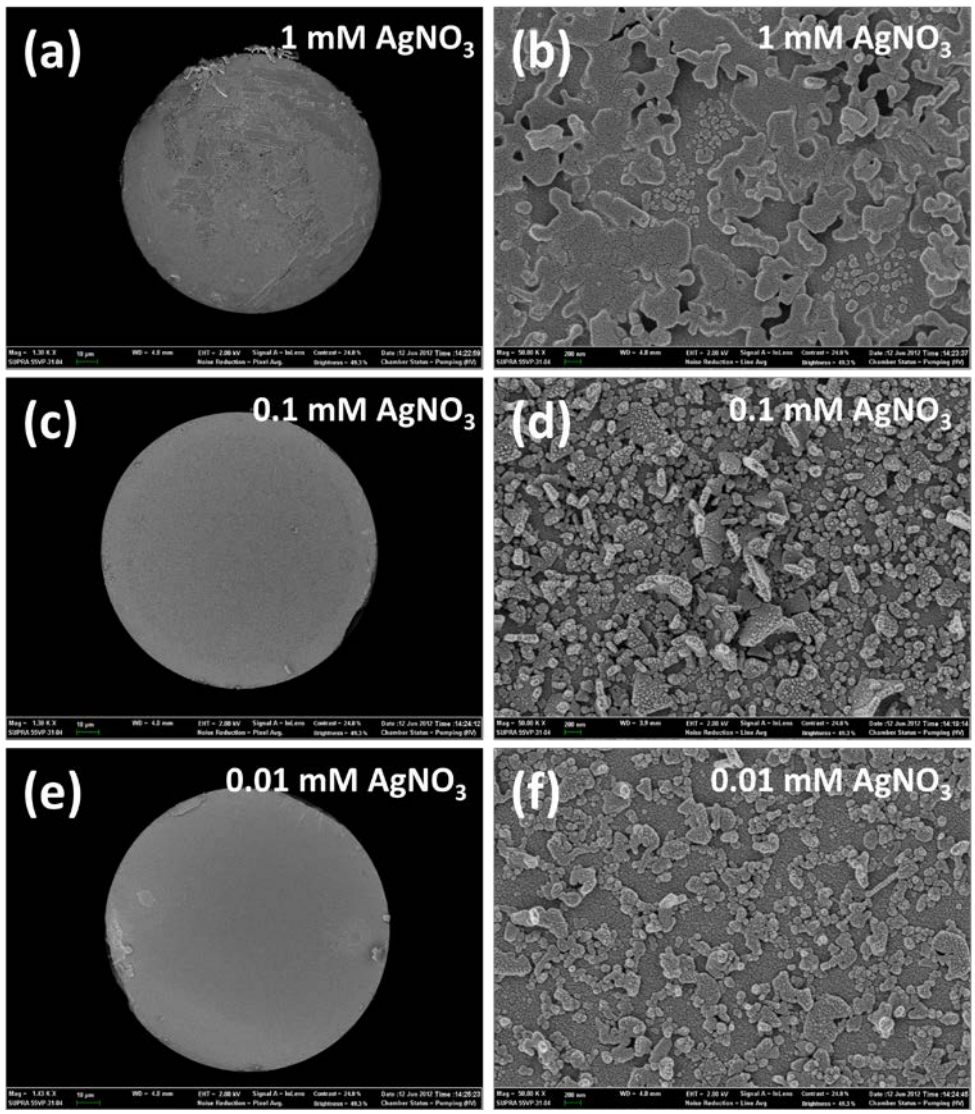

Figure III-21. FE-SEM images of grown Ag NPs on FO one end with different silver nitrate concentrations. The FO one end was treated with a mixed coupling reagent of APMES and TMS (ratio of $1:10^4$) and photo-reduction time was 30 min for all experiments. Mixture of 0.5 ml, 1% (w/v) sodium citrate and 20 ml silver nitrate was used. The concentration of silver nitrate solutions were 1, 0.1 and 0.01 mM for (a), (c) and (d) respectively. (a), (c) and (d) show low magnified image of FO surface and (b), (d) and (f) shows low magnified images respectively.

Figure III-21 shows experimental result of the photo-induced growing of Ag NPs on the FO one end. The FO end surface was treated with a mixed coupling reagent of APMES and TMS with the ratio of $1:10^4$ and photo-reduction time was 30 min for all experiments. Mixture of 0.5 ml, 1% (w/v) sodium citrate and 20 ml silver nitrate was used. The concentration of silver nitrate solutions were 1, 0.1 and 0.01 mM for (a), (c) and (d) respectively. (a), (c) and (d) show low magnified image of FO surface and (b), (d) and (f) shows low magnified images respectively.

From the results, heavily grown Ag NPs on the FO were obtained. The reason of this large growing of Ag NPs, probably caused by the some of the growing condition differences between the glasses based growing. Even thought, when used the same parameters such as photo-reduction time, growth solution concentration, mixed ratio of the substrate, there are many other parameter may affected such as light power of unit area end so on. Therefore, need more experiments to obtain good growing conditions for the FO based photo-induced growing.

Conclusions

We have demonstrated FO based LSPR and SERS simultaneous sensor and its instrument that has the unique ability to detect real-time sensing of molecular binding. The sensor was fabricated using Au NPs and the sensitivity of the FO sensor was defined to measure various refractive indices solutions. In order to detect bio-molecular reaction, antibody-antigen reaction of IFN-γ was used. It is shown that the response of the observed real-time sensorgram delivered the target binding events. In a multiplexing assay, LSPR sensorgram can show the real-time binding process and the SERS signal can differentiate which one of the targets was bound. The concept and method developed in this study can be a basis for developing new multiplex assays for the detection of molecular binding events for bio-sensing applications.

Also we have successfully demonstrated the mono-dispersed growing of Ag NPs directly on glass substrates with photo-inducement in the liquid phase by changing the parameters of the mixed ratio of amine-functional group, photo-reduction time, and concentration of growth solutions. Depending on the SAM layer mixed ratio, the nanoparticles grew on the substrate with various density. The nanoparticles grew only at active

positions of $NH3^{+}$ functional groups of APMES on the substrate. For example, when the ratio of the mixed SAM layer was decreased, the grown nanoparticles showed a higher degree of monomer, mean diameters were increased and surface coverage was decreased.

The mechanism of the growing process is explained as follows. First, by the reductions of Ag^{+} ions to Ag^{0} silver clusters are formed which then grow to small negatively charged spherical seeds. Then small seeds bind to the substrate with different rates. For instance, with 30 min of photo-inducement, the grown nanoparticles were monomers. Then when continuously inducing with light for over 30 min, the number of grown nanoparticles on the substrate increased while the binding rate difference between negative charged seeds to substrate. Therefore, the inter particle distance between growing nanoparticles decreased. So, when the nanoparticles grow further and get larger, they contact each other easily and band together, due to the small distance between the growing nanoparticles. Also the various concentrations of the growth solutions changed the nanoparticle growing rate. The nanoparticles growing rate increased dramatically on the substrate when the growth solutions concentrations were increased; high concentrations of nanoparticle growth solution caused fast growing of nanoparticles. Although, we found the most suitable conditions

for mono-disperse silver nanoparticle growing on substrate to be $1:10^4$, 30 min, and from 0.1 mM to 1 mM for the mixed ratio of substrate silane-coupling reagents of APMES and TMS, photo-reduction time, and concentrations of growth solutions, respectively.

In summary, even though silver nanoparticles can form and grow in solution with photo-illumination, their amount is not as much as the amount grown on surface and their size and shape cannot explain the well-controlled pattern of silver nanoparticles on surface. Silver particles can grow in solution but once they are attached on the amine-functionalized site of surface substantial growing is induced due to intensified local fields close to the silver nanoparticles on surface.

References

1. Haynes, C.L. and R.P. Van Duyne, *Nanosphere lithography: A versatile nanofabrication tool for studies of size-dependent nanoparticle optics.* Journal of Physical Chemistry B, 2001. **105**(24): p. 5599-5611.

2. Grabar, K.C., et al., *PREPARATION AND CHARACTERIZATION OF AU COLLOID MONOLAYERS.* Analytical Chemistry, 1995. **67**(4): p. 735-743.

3. Ulman, A., *Formation and structure of self-assembled monolayers.* Chemical Reviews, 1996. **96**(4): p. 1533-1554.

4. Homola, J., S.S. Yee, and G. Gauglitz, *Surface plasmon resonance sensors: review.* Sensors and Actuators B-Chemical, 1999. **54**(1-2): p. 3-15.

5. Mankiewicz, J., et al., *Genotoxicity of cyanobacterial extracts containing microcystins from Polish water reservoirs as determined by SOS chromotest and comet assay.* Environ Toxicol, 2002. **17**(4): p. 341-50.

6. Vezina, C., A. Kudelski, and S.N. Sehgal, *Rapamycin (AY-22,989), a new antifungal antibiotic. I. Taxonomy of the producing streptomycete and isolation of the active principle.* J Antibiot (Tokyo), 1975. **28**(10): p. 721-6.

7. Binkley, J.F., et al., *Effects of human albumin administration on visceral protein markers in patients receiving parenteral nutrition.* Clin Pharm, 1993. **12**(5): p. 377-9.

8. Langille, M.R., M.L. Personick, and C.A. Mirkin, *Plasmon-mediated syntheses of metallic nanostructures.* Angew Chem Int Ed Engl, 2013. **52**(52): p. 13910-40.

9. Bu, Y. and S.W. Lee, *Optical properties of dopamine molecules with silver nanoparticles as surface-enhanced raman scattering (SERS) substrates at different pH conditions.* J Nanosci Nanotechnol, 2013. **13**(9): p. 5992-6.

10. Hebeish, A., et al., *Development of CMC hydrogels loaded with silver nano-particles for medical applications.* Carbohydr Polym, 2013. **92**(1): p. 407-13.

11. Greeneltch, N.G., et al., *Near-infrared surface-enhanced Raman spectroscopy (NIR-SERS) for the identification of eosin Y: theoretical calculations and evaluation of two different nanoplasmonic substrates.* J Phys Chem A, 2012. **116**(48): p. 11863-9.

12. Grosse, S., L. Evje, and T. Syversen, *Silver nanoparticle-induced cytotoxicity in rat brain endothelial cell culture.* Toxicol In Vitro, 2013. **27**(1): p. 305-13.

13. Ren, W., C. Zhu, and E. Wang, *Enhanced sensitivity of a direct SERS technique for Hg2+ detection based on the investigation of the interaction between silver nanoparticles and mercury ions.* Nanoscale, 2012. **4**(19): p. 5902-9.

14. Steinigeweg, D. and S. Schlucker, *Monodispersity and size control in the synthesis of 20-100 nm quasi-spherical silver nanoparticles by citrate and ascorbic acid reduction in glycerol-water mixtures.* Chem Commun (Camb), 2012. **48**(69): p. 8682-4.

15. Samaranch, L., et al., *Cerebellomedullary Cistern Delivery for AAV-Based Gene Therapy: A Technical Note for Nonhuman Primates.* Hum Gene Ther Methods, 2016. **27**(1): p. 13-6.

16. Sepulveda, B., et al., *LSPR-based nanobiosensors.* Nano Today, 2009. **4**(3): p. 244-251.

17. Mangold, M.A., et al., *Surface plasmon enhanced photoconductance of gold nanoparticle arrays with incorporated alkane linkers.* Applied Physics Letters, 2009. **94**(16): p. -.

18. Praig, V.G., et al., *Localized Surface Plasmon Resonance of Gold Nanoparticle-Modified Chitosan Films for Heavy-Metal Ions Sensing.* Journal of Nanoscience and Nanotechnology, 2009. **9**(1): p. 350-357.

19. Scarano, S., et al., *Surface plasmon resonance imaging for affinity-based biosensors.* Biosensors & Bioelectronics, 2010. **25**(5): p. 957-966.

20. Vezina, C., et al., *Antimycin A fermentation. I. Production and selection of strains.* J Antibiot (Tokyo), 1976. **29**(3): p. 248-64.

21. Homola, J., *OPTICAL-FIBER SENSOR-BASED ON SURFACE-PLASMON EXCITATION.* Sensors and Actuators B-Chemical, 1995. **29**(1-3): p. 401-405.

22. Cervantes-Aviles, P., et al., *Influence of wastewater type on the impact generated by TiO2 nanoparticles on the oxygen uptake rate in activated sludge process.* J Environ Manage, 2016. **190**: p. 35-44.

23. Kudsk, K.A., et al., *Visceral protein response to enteral versus parenteral nutrition and sepsis in patients with trauma.* Surgery, 1994. **116**(3): p. 516-23.

24. Willets, K.A. and R.P. Van Duyne, *Localized surface plasmon resonance spectroscopy and sensing*, in *Annual Review of Physical Chemistry*. 2007, Annual Reviews: Palo Alto. p. 267-297.

25. Hutter, E. and J.H. Fendler, *Exploitation of localized surface plasmon resonance.* Advanced Materials, 2004. **16**(19): p. 1685-1706.

26. Zhao, J., et al., *Localized surface plasmon resonance biosensors.* Nanomedicine, 2006. **1**(2): p. 219-228.

27. Tan, S., et al., *Synthesis of positively charged silver nanoparticles via photoreduction of AgNO3 in branched polyethyleneimine/HEPES solutions.* Langmuir, 2007. **23**(19): p. 9836-43.

28. Sun, R. and R.A. Gu, *[Electrochemical character of gold/silver nanoparticles and SERS studies on benzidine]*. Guang Pu Xue Yu Guang Pu Fen Xi, 2006. **26**(12): p. 2240-3.

29. Yang, J., et al., *Dissolution-recrystallization mechanism for the conversion of silver nanospheres to triangular nanoplates.* J Colloid Interface Sci, 2007. **308**(1): p. 157-61.

30. Pyatenko, A., M. Yamaguchi, and M. Suzuki, *Laser photolysis of silver colloid prepared by citric acid reduction method.* J Phys Chem B, 2005. **109**(46): p. 21608-11.

31. Goulet, P.J., et al., *Surface-enhanced raman scattering on dendrimer/metallic nanoparticle layer-by-layer film substrates.* Langmuir, 2005. **21**(12): p. 5576-81.

32. Srivastava, S.K., R.K. Verma, and B.D. Gupta, *Theoretical modeling of a localized surface plasmon resonance based intensity modulated fiber optic refractive index sensor.* Applied Optics, 2009. **48**(19): p. 3796-3802.

33. Chiappa, A., G.E. Preda, and M. Arposio, *[Influence of the Inflammatory Process on the Metabolism of Lymphatic Tissue. I. Oxygen Consumption and Anaerobic Glycolysis]*. Riv Patol Clin, 1963. **18**: p. 894-8.

34. Hilker, I., et al., *On the influence of oxygen and cell concentration in an SFPR whole cell biocatalytic Baeyer-Villiger oxidation process.* Biotechnol Bioeng, 2006. **93**(6): p. 1138-44.

35. McNay, G., et al., *Surface-Enhanced Raman Scattering (SERS) and Surface-Enhanced Resonance Raman Scattering (SERRS): A Review of Applications.* Applied Spectroscopy, 2011. **65**(8): p. 825-837.

36. Luo, S.C., et al., *Nanofabricated SERS-active substrates for single-molecule to virus detection in vitro: A review.* Biosensors & Bioelectronics, 2014. **61**: p. 232-240.

37. Huh, Y.S., A.J. Chung, and D. Erickson, *Surface enhanced Raman spectroscopy and its application to molecular and cellular analysis.* Microfluidics and Nanofluidics, 2009. **6**(3): p. 285-297.

38. Nie, S.M., *Probing single molecules and single nanoparticles by surface-enhanced Raman scattering.* Abstracts of Papers of the American Chemical Society, 2001. **221**: p. U244-U244.

39. Nie, S.M. and S.R. Emery, *Probing single molecules and single nanoparticles by surface-enhanced Raman scattering.* Science, 1997. **275**(5303): p. 1102-1106.

40. Kneipp, K., et al., *Detection and identification of a single DNA base molecule using surface-enhanced Raman scattering (SERS).* Physical Review E, 1998. **57**(6): p. R6281-R6284.

41. Kneipp, K., et al., *Single molecule detection using surface-enhanced Raman scattering (SERS).* Physical Review Letters, 1997. **78**(9): p. 1667-1670.

42. Kneipp, K., et al., *Ultrasensitive chemical analysis by Raman spectroscopy.* Chemical Reviews, 1999. **99**(10): p. 2957-+.

43. Qian, X.M. and S.M. Nie, *Single-molecule and single-nanoparticle SERS: from fundamental mechanisms to biomedical applications.* Chemical Society Reviews, 2008. **37**(5): p. 912-920.

44. Isola, N.R., D.L. Stokes, and T. Vo-Dinh, *Surface enhanced Raman gene probe for HIV detection.* Analytical Chemistry, 1998. **70**(7): p. 1352-1356.

45. Zhang, C.Y. and L.W. Johnson, *Quantum-dot-based nanosensor for RRE IIB RNA-Rev peptide interaction assay.* Journal of the American Chemical Society, 2006. **128**(16): p. 5324-5325.

46. Salegio, E.A., et al., *Safety study of adeno-associated virus serotype 2-mediated human acid sphingomyelinase expression in the nonhuman primate brain.* Hum Gene Ther, 2012. **23**(8): p. 891-902.

47. Marazuela, M.D. and M.C. Moreno-Bondi, *Fiber-optic biosensors - an overview.* Analytical and Bioanalytical Chemistry, 2002. **372**(5-6): p. 664-682.

48. Leung, A., P.M. Shankar, and R. Mutharasan, *A review of fiber-optic biosensors.* Sensors and Actuators B-Chemical, 2007. **125**(2): p. 688-703.

49. Fan, X.D., et al., *Sensitive optical biosensors for unlabeled targets: A review.* Analytica Chimica Acta, 2008. **620**(1-2): p. 8-26.

50. Wang, X.D. and O.S. Wolfbeis, *Fiber-Optic Chemical Sensors and Biosensors (2013-2015).* Analytical Chemistry, 2016. **88**(1): p. 203-227.

51. Wang, X.D. and O.S. Wolfbeis, *Fiber-Optic Chemical Sensors and Biosensors (2008-2012).* Analytical Chemistry, 2013. **85**(2): p. 487-508.

52. Wolfbels, O.S., *Fiber-optic chemical sensors and biosensors.* Analytical Chemistry, 2008. **80**(12): p. 4269-4283.

53. Wolfbeis, O.S., *Fiber-optic chemical sensors and biosensors.* Analytical Chemistry, 2006. **78**(12): p. 3859-3873.

54. Wolfbeis, O.S., *Fiber optic chemical sensors and biosensors.* Analytical Chemistry, 2000. **72**(12): p. 81r-89r.

55. Byfield, M.P. and R.A. Abuknesha, *Biochemical Aspects of Biosensors.* Biosensors & Bioelectronics, 1994. **9**(4-5): p. 373-400.

56. Rogers, K.R., *Optical-Fiber Biosensors for Herbicide Detection.* Abstracts of Papers of the American Chemical Society, 1995. **209**: p. 34-Agro.

57. Jeong, H.H., et al., *Fabrication of fiber-optic localized surface plasmon resonance sensor and its application to detect antibody-antigen reaction of interferon-gamma.* Optical Engineering, 2011. **50**(12).

58. Jeong, H.H., et al., *Analysis of Fiber-Optic Localized Surface Plasmon Resonance Sensor by Controlling Formation of Gold Nanoparticles and its Bio-Application.* Journal of Nanoscience and Nanotechnology, 2012. **12**(10): p. 7815-7821.

59. Jorgenson, R.C. and S.S. Yee, *A fiber-optic chemical sensor based on surface plasmon resonance.* Sensors and Actuators: B. Chemical, 1993. **12**(3): p. 213-220.

60. Mitsui, K., Y. Handa, and K. Kajikawa, *Optical fiber affinity biosensor based on localized surface plasmon resonance.* Applied Physics Letters, 2004. **85**(18): p. 4231-4233.

61. Stoddart, P.R. and D.J. White, *Optical fibre SERS sensors.* Analytical and Bioanalytical Chemistry, 2009. **394**(7): p. 1761-1774.

62. Doria, G., et al., *Noble Metal Nanoparticles for Biosensing Applications.* Sensors, 2012. **12**(2): p. 1657-1687.

63. Shipway, A.N., E. Katz, and I. Willner, *Nanoparticle arrays on surfaces for electronic, optical, and sensor applications.* Chemphyschem, 2000. **1**(1): p. 18-52.

64. Kelly, K.L., et al., *The optical properties of metal nanoparticles: The influence of size, shape, and dielectric environment.* Journal of Physical Chemistry B, 2003. **107**(3): p. 668-677.

65. Link, S. and M.A. El-Sayed, *Spectral properties and relaxation dynamics of surface plasmon electronic oscillations in gold and silver nanodots and nanorods.* Journal of Physical Chemistry B, 1999. **103**(40): p. 8410-8426.

66. Stiles, P.L., et al., *Surface-Enhanced Raman Spectroscopy*, in *Annual Review of Analytical Chemistry*. 2008, Annual Reviews: Palo Alto. p. 601-626.

67. Barnes, W.L., A. Dereux, and T.W. Ebbesen, *Surface plasmon subwavelength optics.* Nature, 2003. **424**(6950): p. 824-830.

68. Ozbay, E., *Plasmonics: Merging photonics and electronics at nanoscale dimensions.* Science, 2006. **311**(5758): p. 189-193.

69. Herrmann, J.M., *Heterogeneous photocatalysis: fundamentals and applications to the removal of various types of aqueous pollutants.* Catalysis Today, 1999. **53**(1): p. 115-129.

70. Kudo, A. and Y. Miseki, *Heterogeneous photocatalyst materials for water splitting.* Chemical Society Reviews, 2009. **38**(1): p. 253-278.

71. Anker, J.N., et al., *Biosensing with plasmonic nanosensors.* Nature Materials, 2008. **7**(6): p. 442-453.

72. Kudelski, A., et al., *Optically probing the fine structure of a single Mn atom in an InAs quantum dot.* Phys Rev Lett, 2007. **99**(24): p. 247209.

73. Sarikaya, M., et al., *Molecular biomimetics: nanotechnology through biology.* Nature Materials, 2003. **2**(9): p. 577-585.

74. Evanoff, D.D. and G. Chumanov, *Synthesis and optical properties of silver nanoparticles and arrays.* Chemphyschem, 2005. **6**(7): p. 1221-1231.

75. Proniewicz, E., et al., *Raman, surface-enhanced Raman, and density functional theory characterization of (diphenylphosphoryl)(pyridin-2-, -3-, and -4-yl)methanol.* J Phys Chem A, 2014. **118**(30): p. 5614-25.

76. Sebastian, W., et al., *Correlation of antinuclear antibody immunofluorescence patterns with immune profile using line immunoassay in the Indian scenario.* Indian J Pathol Microbiol, 2010. **53**(3): p. 427-32.

77. McFarland, A.D. and R.P. Van Duyne, *Single silver nanoparticles as real-time optical sensors with zeptomole sensitivity.* Nano Letters, 2003. **3**(8): p. 1057-1062.

78. Tao, A.R., S. Habas, and P.D. Yang, *Shape control of colloidal metal nanocrystals.* Small, 2008. **4**(3): p. 310-325.

79. Xu, Z.M., et al., *Synthesis of Self-assembled Noble Metal Nanoparticle Chains Using Amyloid Fibrils of Lysozyme as Templates.* Nanomaterials and Nanotechnology, 2016. **6**.

80. Fazio, E., et al., *Laser Controlled Synthesis of Noble Metal Nanoparticle Arrays for Low Concentration Molecule Recognition.* Micromachines, 2014. **5**(4): p. 1296-1309.

81. An, H.H., et al., *Structure of solid-supported lipid membrane probed by noble metal nanoparticle deposition.* Biochimica Et Biophysica Acta-Biomembranes, 2012. **1818**(11): p. 2884-2891.

82. Zhang, Y.J., et al., *Synthesis, properties, and optical applications of noble metal nanoparticle-biomolecule conjugates.* Chinese Science Bulletin, 2012. **57**(2-3): p. 238-246.

83. Porter, L.A., et al., *Controlled electroless deposition of noble metal nanoparticle films on germanium surfaces.* Nano Letters, 2002. **2**(10): p. 1067-1071.

84. Jensen, T., et al., *Electrodynamics of noble metal nanoparticles and nanoparticle clusters.* Journal of Cluster Science, 1999. **10**(2): p. 295-317.

85. Grzelczak, M., et al., *Shape control in gold nanoparticle synthesis.* Chemical Society Reviews, 2008. **37**(9): p. 1783-1791.

86. Koehler, J.M., N. Visaveliya, and A. Knauer, *Controlling formation and assembling of nanoparticles by control of electrical charging, polarization, and electrochemical potential.* Nanotechnology Reviews, 2014. **3**(6): p. 553-568.

87. Morales, N., et al., *Influence of dissolved oxygen concentration on the start-up of the anammox-based process: ELAN(R).* Water Sci Technol, 2015. **72**(4): p. 520-7.

88. Mowatt-Larssen, C.A., et al., *Comparison of tolerance and nutritional outcome between a peptide and a standard enteral formula in critically ill, hypoalbuminemic patients.* JPEN J Parenter Enteral Nutr, 1992. **16**(1): p. 20-4.

89. Piergies, N., et al., *Fourier transform infrared and Raman and surface-enhanced Raman spectroscopy studies of a novel group of boron analogues of aminophosphonic acids.* J Phys Chem A, 2012. **116**(40): p. 10004-14.

90. Mayer, A.B.R., *Formation of noble metal nanoparticles within a polymeric matrix: nanoparticle features and overall morphologies.* Materials Science & Engineering C-Biomimetic and Supramolecular Systems, 1998. **6**(2-3): p. 155-166.

91. Bjerneld, E.J., F. Svedberg, and M. Kall, *Laser-induced growth and deposition of noble-metal nanoparticles for surface-enhanced Raman scattering.* Nano Letters, 2003. **3**(5): p. 593-596.

92. Canamares, M.V., et al., *Ag nanoparticles prepared by laser photoreduction as substrates for in situ surface-enhanced raman scattering analysis of dyes.* Langmuir, 2007. **23**(9): p. 5210-5215.

93. Niidome, Y., et al., *Laser-induced deposition of gold nanoparticles onto glass substrates in cyclohexane.* Nano Letters, 2001. **1**(7): p. 365-369.

94. Zheng, X.L., et al., *Laser-induced growth of monodisperse silver nanoparticles with tunable surface plasmon resonance properties and a wavelength self-limiting effect.* Journal of Physical Chemistry C, 2007. **111**(41): p. 14962-14967.

95. Courrol, L.C., F. Silva, and L. Gomes, *A simple method to synthesize silver nanoparticles by photo-reduction.* Colloids and Surfaces a-Physicochemical and Engineering Aspects, 2007. **305**(1-3): p. 54-57.

96. Hodak, J.H., et al., *Laser-induced inter-diffusion in AuAg core-shell nanoparticles.* Journal of Physical Chemistry B, 2000. **104**(49): p. 11708-11718.

97. Mafune, F., et al., *Growth of gold clusters into nanoparticles in a solution following laser-induced fragmentation.* Journal of Physical Chemistry B, 2002. **106**(34): p. 8555-8561.

98. Sakamoto, M., M. Fujistuka, and T. Majima, *Light as a construction tool of metal nanoparticles: Synthesis and mechanism.* Journal of Photochemistry and Photobiology C-Photochemistry Reviews, 2009. **10**(1): p. 33-56.

99. Tolaymat, T.M., et al., *An evidence-based environmental perspective of manufactured silver nanoparticle in syntheses and applications: A systematic review and critical appraisal of peer-reviewed scientific papers.* Science of the Total Environment, 2010. **408**(5): p. 999-1006.

100. Tsuji, T., N. Watanabe, and M. Tsuji, *Laser induced morphology change of silver colloids: formation of nano-size wires.* Applied Surface Science, 2003. **211**(1-4): p. 189-193.

101. Zheng, X.L., et al., *Photochemical modification of an optical fiber tip with a silver nanoparticle film: A SERS chemical sensor.* Langmuir, 2008. **24**(8): p. 4394-4398.

102. Link, S. and M.A. El-Sayed, *Shape and size dependence of radiative, non-radiative and photothermal properties of gold nanocrystals.* International Reviews in Physical Chemistry, 2000. **19**(3): p. 409-453.

103. Takahashi, H., et al., *Effects of capping thiols on the laser-induced fusion of gold nanoparticles and deposition onto glass substrates in cyclohexane.* Colloids and Surfaces a-Physicochemical and Engineering Aspects, 2004. **247**(1-3): p. 105-113.

104. Ravula, S., et al., *Sunlight-assisted route to antimicrobial plasmonic aminoclay catalysts.* Nanoscale, 2015. **7**(1): p. 86-91.

105. Liu, Y., et al., *Localized and propagating surface plasmon co-enhanced Raman spectroscopy based on evanescent field excitation.* Chemical Communications, 2011. **47**(13): p. 3784-3786.

106. Izal-Azcarate, A., et al., *Isolation, culture and characterization of adult carotid body-derived cells.* Respir Physiol Neurobiol, 2009. **167**(2): p. 201-7.

107. Sukumaran, S., W. Sebastian, and A. Gopalakrishnan, *Population genetic structure of Indian oil sardine, Sardinella longiceps along Indian coast.* Gene, 2016. **576**(1 Pt 2): p. 372-8.

108. Xuan, X.Y., et al., *A Long-Range Surface Plasmon Resonance/Probe/Silver Nanoparticle (LRSPR-P-NP) Nanoantenna Configuration for Surface-Enhanced Raman Scattering.* Journal of Physical Chemistry Letters, 2012. **3**(19): p. 2773-2778.

109. Meyer, S.A., E.C. Le Ru, and P.G. Etchegoin, *Combining Surface Plasmon Resonance (SPR) Spectroscopy with Surface-Enhanced Raman Scattering (SERS).* Analytical Chemistry, 2011. **83**(6): p. 2337-2344.

110. Jeong, H.H., et al., *Real-time label-free immunoassay of interferon-gamma and prostate-specific antigen using a Fiber-Optic Localized Surface Plasmon Resonance sensor.* Biosensors & Bioelectronics, 2013. **39**(1): p. 346-351.

111. Canamares, M.V., et al., *Comparative study of the morphology, aggregation, adherence to glass, and surface-enhanced Raman scattering activity of silver nanoparticles prepared by chemical reduction of Ag+ using citrate and hydroxylamine*. Langmuir, 2005. **21**(18): p. 8546-53.

요 약

바이오 응용을 위한 LSPR 과 SERS 동시측정방법: 광학 시스템과 센서 기판에 대해서

노로에르덴

협동과정 나노과학기술 전공

서울대학교 대학원

바이오 분자의 검출을 위해, 다양한 방법을 이용한 바이오 센서들이 개발되어 왔으며 각각의 바이오 센서들은 기기 적인 측면에서 다양한 장점과 차이점 들을 가지고 있다. 그러한 연구 속에서, 본 연구에서는 광섬유 기반의 바이오 센서를 개발하고자 한다. 광섬유 기반의 바이오센서는 다양한 장점들을 가지고 있으며 특히 광섬유 기반의 바이오센서는 항원-항체 반응의 국소 표면 플라즈몬 (localized surface plasmon resonance, LSPR)과 표면 증강 라만 산란 (Surface-enhanced Raman scattering, SERS) 동시 측정 및 실시간 측정이 가능하며 이를 기반으로 본 연구에서는 표적 물질 없이 인터페론-감마(IFN-γ)의 항원-항체 반응을 바이오 분야의 응용을 위한 개념 증명 형태로 성공적인 실험 수행을 진행하였다.

챕터 1 에서는 본 연구의 간단한 이론, 기본 법칙 및 연구 목적에 대해서 간략하게 제시하였다. 또한 최근 기술 중에서 바이오 분자 검출을 위해 널리 사용되는 것들에 대한 예시와 함께 간단한 논의를 첨부하였다.

챕터 2 에서는 광섬유 기반의 바이오 분자 검출을 위한 LSPR 및 SERS 동시 측정 시스템의 개발에 대해서 기술하였다. 우선 광섬유 말단 표면에 50 nm 정도 크기를 가지는 금 나노 입자를 표면 화학 처리를 이용하여 고정시켰으며 LSPR 및 SERS 동시 측정을 위해 분광학적 시스템을 개발하였다. 개발한 시스템을 이용하여 금 나노 입자가 도입된 광섬유의 LSPR 신호의 민감도 및 재현 가능성을 살펴보기 위해 굴절률에 따른 신호 변화를 측정하였으며 또한 SERS 신호의 민감도 및 재현 가능성 여부를 확인하기 위해 4-aminothiophenol (4-ATP)를 도입하여 SERS 신호의 여부를 확인하였다. 이를 기반으로 IFN-γ 의 실시간 LSPR 신호 변화 및 4-ATP 의 SERS 스펙트럼의 변화를 동시 측정 하였으며 이를 통해 생물학적 응용의 가능성을 확인하였다.

바이오 분자 검출을 위한 SPR 및 SERS 센서를 구현하기 위해서는 유리 기판 혹은 광섬유 표면에 귀금속 나노 입자가 도입되어야 한다. 현재 대부분의 용액 기반의 연구에서는 기판 표면의 나노 입자 배열의 불균일성으로 인해 신호의 민감도나 재현성이 낮은 경우가 많으며 이를 극복하기 위해 도입하는 전자빔을 이용한 리소그래피 방법이나 진공 스퍼터링 등을 이용하여 기판 표면을 처리하는 방법들은 가격적인 측면에서 비싸고 복잡한 기기들이 필요한 경우가 대부분이다. 이러한 표면 기판의 나노

입자의 처리하는 방법들이 가지고 있는 여러 단점을 극복하는 대안으로 기판 표면에 직접적으로 나노 입자를 광 유도 반응을 이용해 만드는 것이 제시되었으나 이러한 방법 역시 현재 연구 수준에서는 여전히 균일도가 낮은 모습들을 보이고 있다. 이를 극복하기 위해 챕터 3 에서는 유리 기판 표면에 은 나노 입자를 단분산 시킬 수 있는 간단한 방법 개발에 대해서 기술하였다. 우선 균일한 유리 기판 표면처리를 위하여 유리 기판 표면에 아민 작용기와 알킬 그룹을 일정한 비율로 도입하였다. 또한 빛을 조명하는 시간 역시 조절하였으며 성장 용액 속의 질산은과 시트르산 나트륨의 농도를 조절하여 기판 표면에서 성장하는 나노 입자의 크기 및 단 분산성을 조절하였다. 이러한 단 분산성은 전계 방출 주사 전자 현미경(Field-emission scanning electron microscopy) 과 암시야(Dark-field) 현미경을 이용하여 확인하였다. 이를 기반으로 실험 결과에 대한 광 유도 반응에 대한 이론적인 메커니즘을 규명하였다.

주요어 : 광섬유, 국소 표면 플라즈몬 공명, 표면 증강 라만 산란, 동시 측정, 금 나노입자, 은 나노입자, 인터페론 감마, 광-환원 성장, 혼합 자기조립 단일층, 유리 기판

학 번 : 2006-30675